Copy 6
RM L53H13

NACA

RESEARCH MEMORANDUM

THE AERODYNAMIC CHARACTERISTICS AT TRANSONIC SPEEDS OF AN ALL-MOVABLE, TAPERED, 45° SWEPTBACK, ASPECT-RATIO-4 TAIL DEFLECTED ABOUT A SKEWED HINGE AXIS AND EQUIPPED WITH AN INSET UNBALANCING TAB

By James M. Watson

Langley Aeronautical Laboratory
Langley Field, Va.

NATIONAL ADVISORY COMMITTEE
FOR AERONAUTICS

WASHINGTON
September 29, 1953

NACA RM L53H13

NATIONAL ADVISORY COMMITTEE FOR AERONAUTICS

RESEARCH MEMORANDUM

THE AERODYNAMIC CHARACTERISTICS AT TRANSONIC SPEEDS OF AN ALL-MOVABLE, TAPERED, 45° SWEPTBACK, ASPECT-RATIO-4 TAIL DEFLECTED ABOUT A SKEWED HINGE AXIS AND EQUIPPED WITH AN INSET UNBALANCING TAB

By James M. Watson

SUMMARY

An investigation was made at transonic speeds in the Langley high-speed 7- by 10-foot tunnel to determine the hinge-moment, lift, and pitching-moment characteristics of an overbalanced all-movable tail surface deflected about a skewed hinge axis and equipped with an inset unbalancing tab. The aspect-ratio-4 tail surface had a sweepback of 45° at the quarter-chord line, a taper ratio of 0.6, and an NACA 65A006 airfoil section parallel to the free stream. The investigation was made through the transonic speed range by testing in the high-velocity flow field generated over the curved surface of a bump placed on the floor of the tunnel. The lift effectiveness of the tab was positive through the Mach number range investigated, but, like other flap-type controls, its effectiveness was materially reduced through the transonic speed range. The tab effectiveness in producing tail hinge moment changed only slightly with Mach number and the ratio of tab deflection to tail deflection required to balance the hinge moments resulting from deflection of the tail showed a large decrease at transonic speeds as a result of the rearward shift of the centers of pressure of the tail. Some method by which the ratio of the tab deflection to tail deflection could be varied with tail hinge moment would be required to provide satisfactory balancing of the hinge moments of the tail throughout the Mach number range.

The gap at the root-chord line of the tail caused by deflection of the all-movable tail decreased the lift-curve slope and maximum lift at 20° and 30° tail deflection but had little effect on the hinge-moment characteristics.

INTRODUCTION

For several years designers have been aware of the more desirable characteristics of the all-movable control over the conventional flap-type control (see refs. 1 and 2). The all-movable control is even more desirable at transonic speed because the decrease of effectiveness of the all-movable tail is less than that of the flap-type of control. Both controls, however, show large rearward shifts in the center of pressure in the transonic speed range which make control balancing difficult. A recent investigation has shown (ref. 1) that the effects of the center-of-pressure movement on the balancing characteristics may be materially reduced on an all-movable tail by pivoting the tail about a skewed axis near the locus of centers of pressure. This arrangement gives a more desirable variation of hinge-moments with angle of attack and Mach number than one in which the axis is normal to the plane of symmetry. Although the configuration of reference 1 gave relatively low hinge-moment coefficients through the low lift coefficient range, even closer balancing must be obtained in order to achieve unboosted pilot operation of the controls.

The present investigation deals with an all-movable control surface similar to the one described above, that is, one pivoted about a skewed hinge axis. The skewed axis was chosen from the center-of-pressure data presented in reference 1, such that the hinge moments of the tail would be overbalanced at low Mach numbers and about balanced at transonic Mach numbers. The hinge moments of the tail could then be balanced by installing an inset unbalancing tab whose effectiveness at low Mach numbers is sufficient to balance the hinge moments of the tail although the effectiveness of the tab would be expected to decrease rapidly in the transonic speed range (ref. 3). This control arrangement has the additional advantage that the tab lift is added to the tail lift instead of being subtracted from it as with the conventional balancing tab.

The present investigation presents the lift and moment characteristics of an aspect-ratio-4.0 tail, sweptback 45° at the quarter-chord line and pivoted about an axis sweptback 55.5° and passing through the leading edge of the root-chord line. The tail was equipped with a 20-percent-chord, 50-percent-semispan inset unbalancing tab. The effect of the gap at the root-chord line caused by deflection of the tail has also been investigated. The Mach number range of the tests is from 0.61 to 1.21, obtained by the transonic-bump technique.

SYMBOLS

The forces and moments on the tail are presented relative to the axes shown in figure 1.

[redacted]

C_L lift coefficient, $\frac{\text{Twice lift of semispan model}}{qS}$

C_m pitching-moment coefficient referred to leading edge of root-chord line (see fig. 1), $\frac{\text{Twice pitching moment of semispan model}}{qS\bar{c}}$

C_h hinge-moment coefficient about hinge line (see figs. 1 and 2), $\frac{\text{Twice hinge moment of semispan model}}{qS\bar{c}}$

q effective dynamic pressure over span of model, $\frac{1}{2}\rho V^2$, lb/sq ft

S twice area of semispan model, 0.125 sq ft

$\bar{c}$ mean aerodynamic chord, $\frac{2}{S}\int_0^{b/2} c^2 dy$ = 0.1805 ft on model

c local wing chord, ft

b twice span of semispan model, 0.707 ft

y spanwise distance from plane of symmetry, ft

ρ mass density of air, slugs/cu ft

V average free-stream velocity, fps

M effective Mach number over span of model

M_a average chordwise local Mach number

M_l local Mach number

R Reynolds number of model based on $\bar{c}$

α angle of attack (measured in the plane of symmetry), deg

A aspect ratio, $\frac{b^2}{S}$ = 4.0 on model

λ taper ratio, 0.6 on model

δ deflection of model about hinge axis swept back 55.5° and passing through the leading edge of root-chord line, deg (positive deflection shown in fig. 1)

[redacted]

δ_t deflection of inset unbalancing tab about 80-percent-chord line, deg (positive deflection shown in fig. 1)

Λ_{HL} angle of sweep of the hinge line, 55.5°

$\delta \cos \Lambda_{HL}$ change in angle of attack at the root-chord line caused by change in tail deflection about the hinge line

$\alpha + \delta \cos \Lambda_{HL}$ resultant change in angle of attack, deg

$$c_{h_\delta} = \frac{\partial c_h}{\partial \delta}$$

$$c_{L_\delta} = \frac{\partial c_L}{\partial \delta}$$

$$c_{h_{\delta_t}} = \frac{\partial c_h}{\partial \delta_t}$$

$$c_{L_{\delta_t}} = \frac{\partial c_L}{\partial \delta_t}$$

MODEL AND APPARATUS

The all-movable tail used in the investigation has an aspect ratio of 4, a taper ratio of 0.6, a sweepback of 45° at the quarter-chord line, and an NACA 65A006 airfoil section parallel to the free air stream. The tail was mounted on the transonic bump and was the same as that investigated in reference 1. The tail was made of steel to the plan-form dimensions shown in figure 2.

The hinge axis of the all-movable tail was swept back 55.5° and passed through the leading edge of the root-chord line of the tail (see fig. 2). At a given tail deflection, the model was restrained from rotating about the hinge axis by an electrical strain-gage beam secured to a shaft extending the hinge axis through the surface of the bump.

A 20-percent-chord, 50-percent-semispan, inset tab was made in the tail surface by cutting a 1/32-inch groove in both surfaces of the tail along the 80-percent-chord line as shown in figure 3. Experience has shown that the grooves facilitate setting the tab deflection angle and have a negligible effect on deflection under load. The grooves were filled and faired smoothly.

[redacted]

The tail was so arranged that the gap between the root of the tail and the bump surface was only about 1/16 inch at 0° tail deflection (see fig. 4), and opened up as the tail was deflected. The gap between the butt of the model (fig. 4) and the turntable of the bump was sealed by a thin sponge seal to eliminate air flow around the butt of the model into the balance chamber in the bump.

Force and moment measurements were obtained on an electrical-strain-gage balance system.

TESTS

The all-movable tail was tested in the Langley high-speed 7- by 10-foot tunnel by utilizing the flow field generated over the transonic bump to obtain Mach numbers from 0.61 to 1.21. The transonic-bump technique is described in reference 4. Typical contours showing the Mach number distribution over the bump in the vicinity of the model are shown in figure 5. Effective test Mach numbers were obtained from contour charts similar to those shown in figure 5 by the relationship

$$M = \frac{2}{S}\int_0^{b/2} cM_a \, dy$$

For these tests a Mach number gradient outside the boundary layer of generally less than 0.03 was obtained below a Mach number of 0.95 and the gradient increased to about 0.06 at the higher test Mach numbers. The variation of Reynolds number with Mach number is presented in figure 6.

The angles of attack were measured in a plane perpendicular to a normal axis through the leading edge of the root-chord line (the xz-plane, see fig. 1), and the tail deflections were measured in a plane perpendicular to the 55.5° sweptback hinge line. The model was symmetrical; therefore, in order to reduce the number of model changes and the tunnel time, the force and moment measurements were taken through an angle-of-attack range from -30° to 30° and at tail deflections from 0° to 30°. These measurements could then be considered, with due regard to sign, to be equivalent to the measurements that would be obtained through an angle-of-attack range from 0° to 30° and at tail deflections from -30° to 30°.

The inset tab was investigated at deflections of -10° to 10° normal to the tab hinge line through an angle-of-attack range of -30° to 30° at tail deflections of 0°, 10°, and 20°.

[redacted]

In view of the small size of the tail relative to the tunnel test section, jet-boundary and blockage corrections were believed to be insignificant and were not applied to the data.

RESULTS AND DISCUSSION

The lift and hinge-moment characteristics of an all-movable, 45° sweptback tail pivoted about a skewed hinge axis are presented in figures 7, 8, and 9 as a function of inset tab deflection for several angles of attack, Mach numbers, and tail deflections. The lift, pitching-moment, and hinge-moment coefficients have also been plotted against the resultant change in angle of attack, $\alpha + \delta \cos \Lambda_{HL}$ in figure 10 at a tab deflection of 0°. The pitching-moment and hinge-moment coefficients for various tab deflections have been plotted against lift coefficient at various Mach numbers and tail deflections in figures 11, 12, and 13.

The control characteristics of the all-movable tail have been summarized in figure 14. The lift and hinge-moment parameters of the tail are based on the incremental value of the coefficients between $\delta = 0°$ and $\delta = 10°$ at $\alpha = \delta_t = 0°$. The tab parameters are based on the average slope of the coefficient curves between $\delta_t = \pm 10°$ at $\alpha = \delta = 0°$.

The parameter C_{h_δ} (fig. 14) indicates that the all-movable tail is overbalanced throughout the Mach number range, but, as was expected from the present hinge-axis location and from the center-of-pressure movement shown in reference 1, the overbalance was small at a Mach number of 1.00 or above. The overbalanced condition is limited to values of $\alpha + \delta \cos \Lambda_{HL}$ of about ±6° at subsonic Mach numbers but covers a greater range of $\alpha + \delta \cos \Lambda_{HL}$ above $M = 1.00$. The tab effectiveness in producing tail hinge moments $C_{h_{\delta_t}}$ shows only slight increase through the Mach number range. The ratio of the two parameters $C_{h_\delta}/C_{h_{\delta_t}}$ is the amount of tab deflection per degree of tail deflection δ_t/δ required to balance out the hinge moments resulting from deflection of the tail. Although the tab effectiveness in producing tail hinge moment changed only slightly with Mach number, the ratio of δ_t/δ required to balance the hinge moments resulting from deflection of the tail showed a large decrease at transonic speeds as a result of the rearward shift of the centers of pressure of the tail. The variation of the ratio δ_t/δ with Mach number indicates that a spring tab, or some other method by which the linkage or ratio of δ_t/δ could be varied with the hinge moment, would be required to provide staisfactory balancing of the hinge moments of the tail throughout the Mach number range investigated.

[redacted]

The lift effectiveness of the tab as given by the parameter $C_{L_{\delta_t}}$ (fig. 14) is positive throughout the Mach number range and varies with Mach number much like any other flap-type control which usually shows a large reduction in effectiveness in passing through a Mach number of 1.00. The value of $C_{L_{\delta_t}}$ at $M = 1.21$ is only about 45 percent of the value obtained at $M = 0.61$.

The advantage of using an overbalanced control and an unbalancing tab is apparent in figure 14 where the net lift parameter $\left(C_{L_\delta}\right)_{C_h=0}$ is given by the following equation:

$$\left(C_{L_\delta}\right)_{C_h=0} = C_{L_\delta} + C_{L_{\delta_t}}\left(\frac{\delta_t}{\delta}\right)$$

and is greater than the tail lift parameter C_{L_δ}. It should be remembered, however, that these parameters apply only over the range of deflection at which the slopes were measured, and at other values of $\alpha + \delta \cos \Lambda_{HL}$ (fig. 10) the tab may be required to provide balance rather than unbalance with a resulting loss in lift effectiveness.

A comparison of the variation of the hinge-moment characteristics with Mach number of an all-movable tail pivoted about a normal axis at $0.25\bar{c}$ (from ref. 1), pivoted about a skewed axis on the 20-percent-chord line (from ref. 1), and pivoted about an axis swept back 55.5° (from the data of this report) is presented in figure 15. These data show that the hinge moments of the all-movable tail pivoted about an axis swept back 55.5° were overbalanced through the Mach number range, while the hinge moments of the all-movable tail pivoted about the other axes were underbalanced.

The gap at the root-chord line resulting from deflection of the tail surface does not appear to have much effect on the hinge-moment characteristics as is indicated in figure 10. These data do show a decrease in lift-curve slope, particularly at $\delta = 30°$, and a decrease in maximum lift coefficient above about 10° tail deflection.

CONCLUSIONS

An investigation was made in the Langley high-speed 7- by 10-foot tunnel to determine the effect of an inset unbalancing tab on the hinge moments and aerodynamic characteristics of an overbalanced all-movable,

45° sweptback, aspect-ratio-4, taper-ratio-0.6 tail deflected about a skewed hinge axis. The following conclusions may be drawn from the data:

1. The lift effectiveness of the tab was positive through the Mach number range investigated, but, like other flap-type controls, its effectiveness was materially reduced through the transonic speed range.

2. Although the tab effectiveness in producing tail hinge moment changed only slightly with Mach number, the ratio of tab deflection to tail deflection required to balance the hinge moments resulting from deflection of the tail showed a large decrease at transonic speeds as a result of the rearward shift of the centers of pressure of the tail.

3. Some method by which the ratio of the tab deflection to tail deflection could be varied with tail hinge moment would be required to provide satisfactory balancing of the hinge moments of the tail throughout the Mach number range.

Langley Aeronautical Laboratory,
National Advisory Committee for Aeronautics,
Langley Field, Va., July 30, 1953.

REFERENCES

1. Hammond, Alexander D., and Watson, James M.: The Aerodynamic Characteristics at Transonic Speeds of an All-Movable, Tapered, 45° Sweptback, Aspect-Ratio-4 Tail Surface Deflected About a Skewed Hinge Axis. NACA RM L52D28, 1952.

2. Mitchell, Jesse L.: The Static and Dynamic Longitudinal Stability Characteristics of Some Supersonic Aircraft Configurations. NACA RM L52A10a, 1952.

3. Lockwood, Vernard E., and Fikes, Joseph E.: Preliminary Investigation at Transonic Speeds of the Effect of Balancing Tabs on the Hinge-Moment and Other Aerodynamic Characteristics of a Full-Span Flap on a Tapered 45° Sweptback Wing of Aspect Ratio 3. NACA RM L52A23, 1952.

4. Donlan, Charles J., Myers, Boyd C., II, and Mattson, Axel T.: A Comparison of the Aerodynamic Characteristics at Transonic Speeds of Four Wing-Fuselage Configurations as Determined From Different Test Techniques. NACA RM L50H02, 1950.

[redacted]

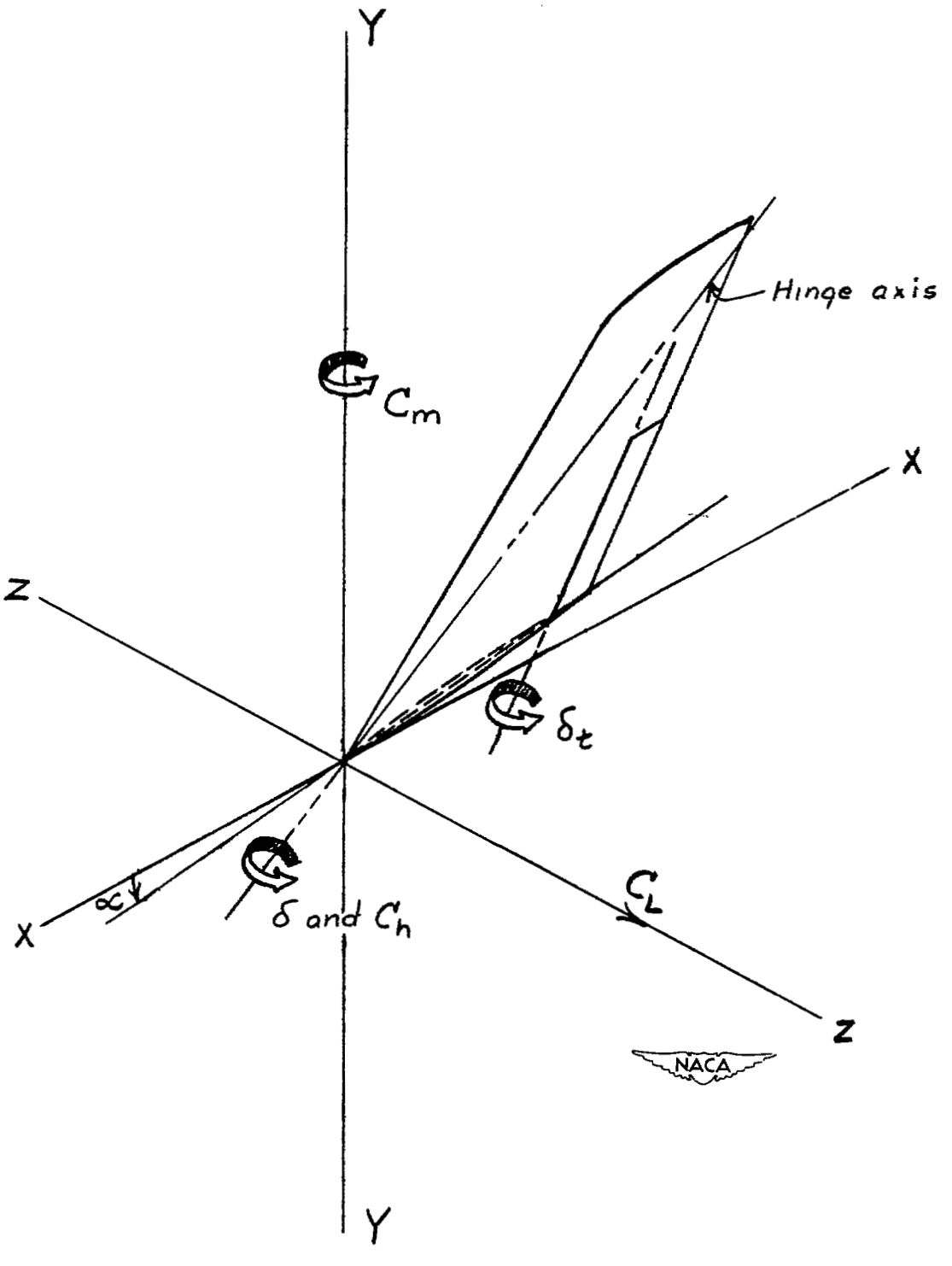

Figure 1.- System of axes, tail hinge moments, and deflections. Positive directions of forces, moments, and deflections are indicated by arrows.

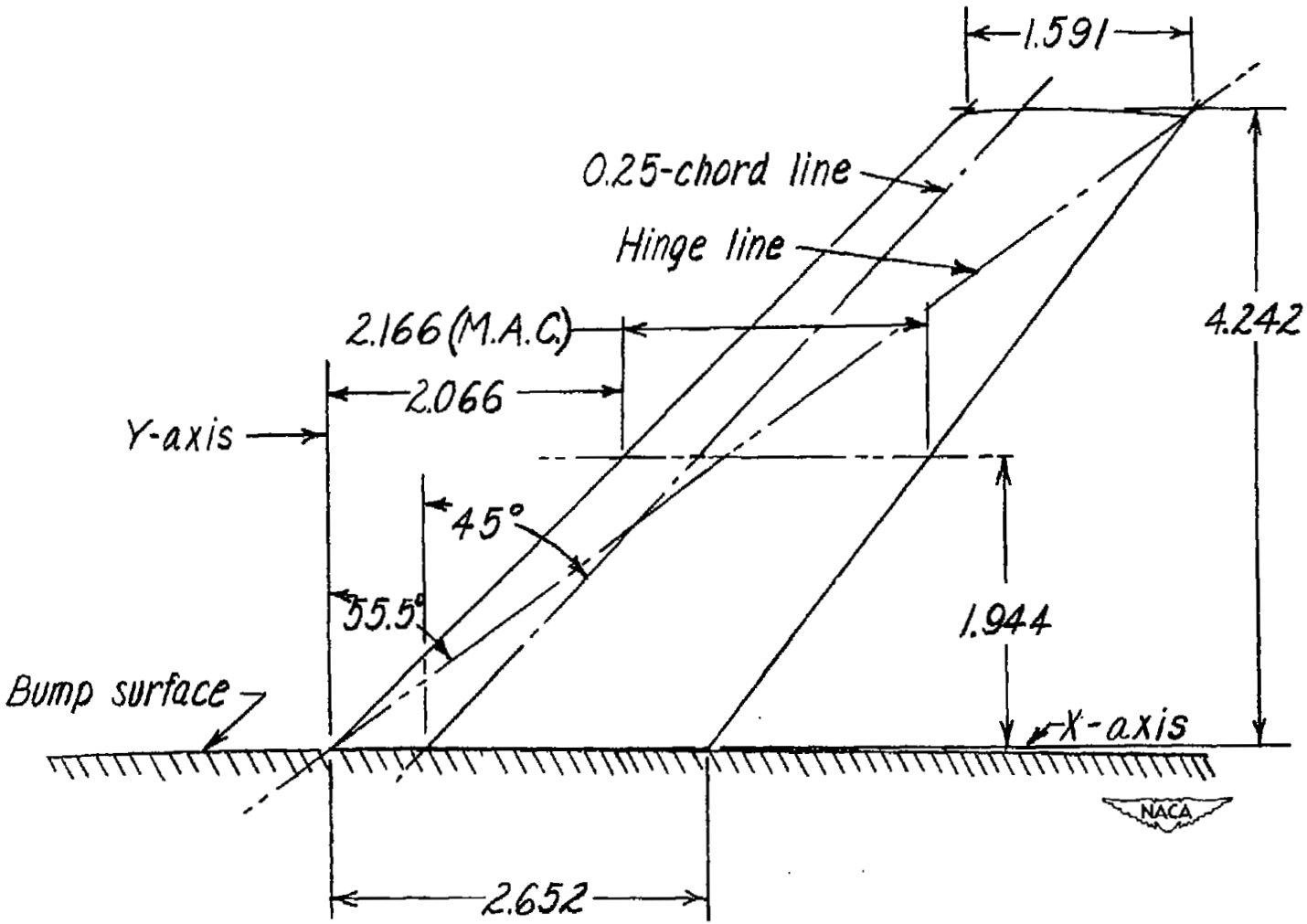

Figure 2.- Plan form and dimensions of the aspect-ratio-4, taper-ratio-0.6, 45° sweptback all-movable tail. All dimensions are in inches unless otherwise noted.

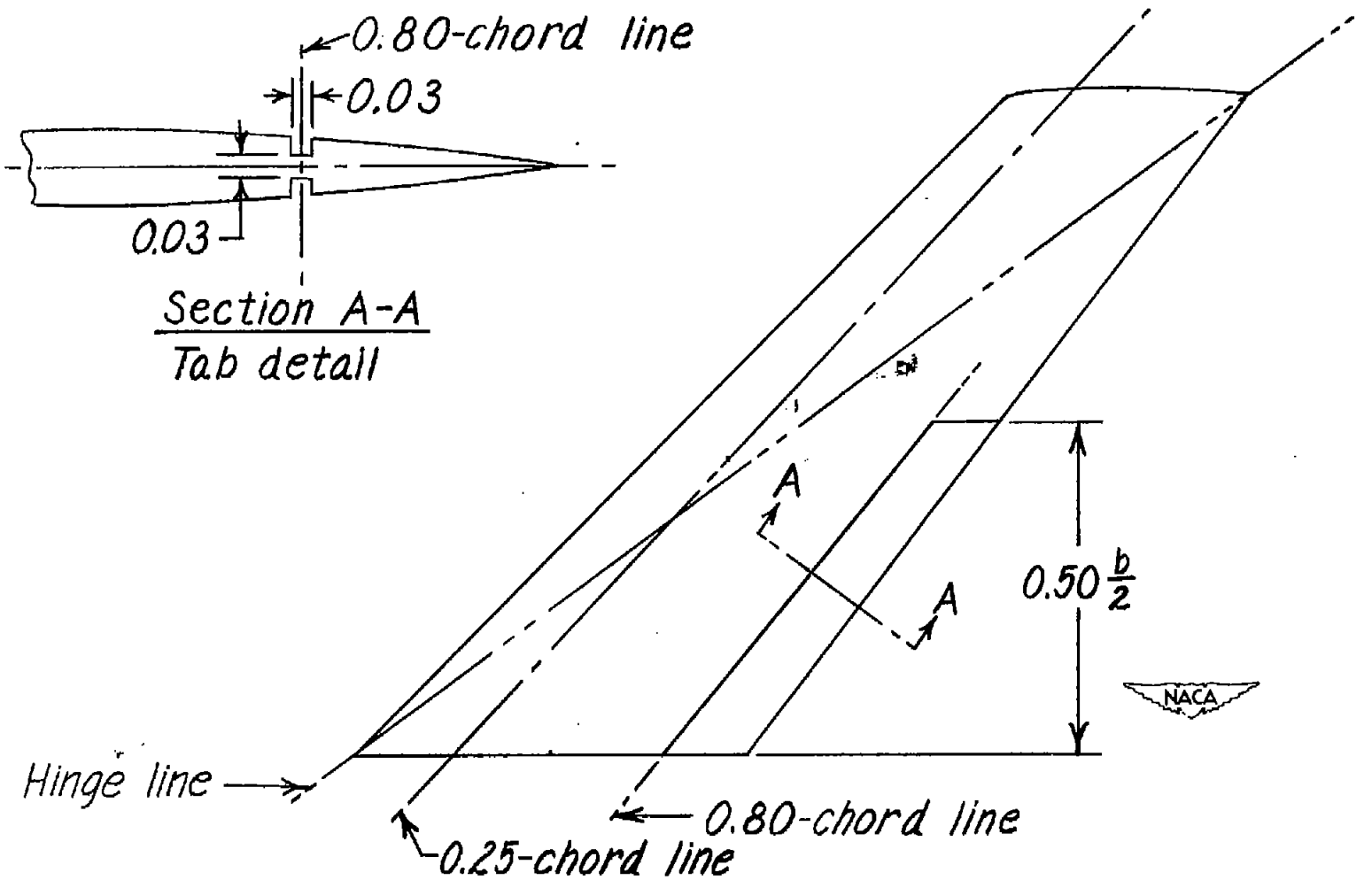

Figure 3.- Location and dimensions of the inset tab investigated on the all-movable tail. All dimensions in inches unless otherwise noted.

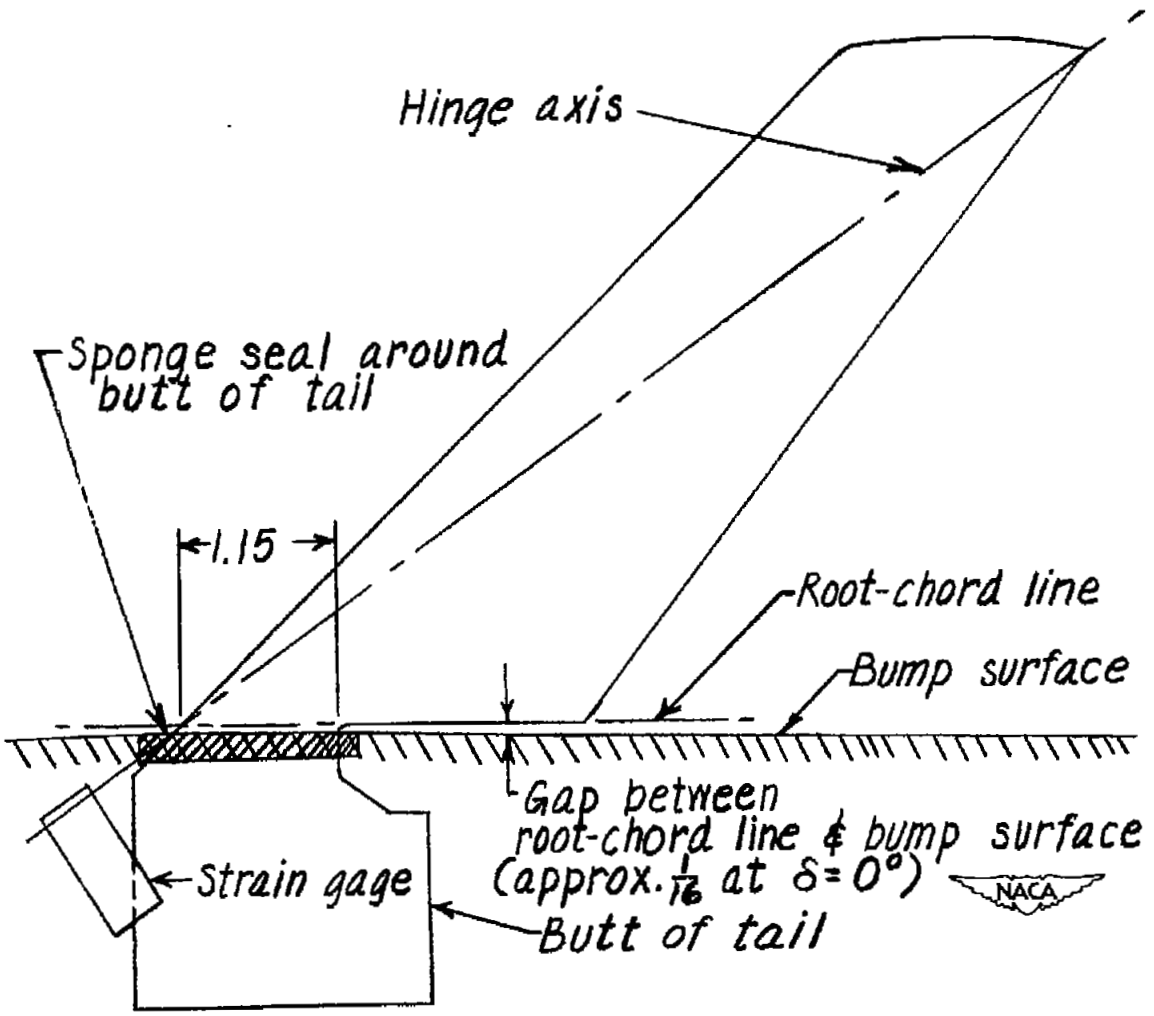

Figure 4.- The arrangement of the sponge seal and the gap between the root-chord line of the all-movable tail and the bump surface. All dimensions in inches unless otherwise noted.

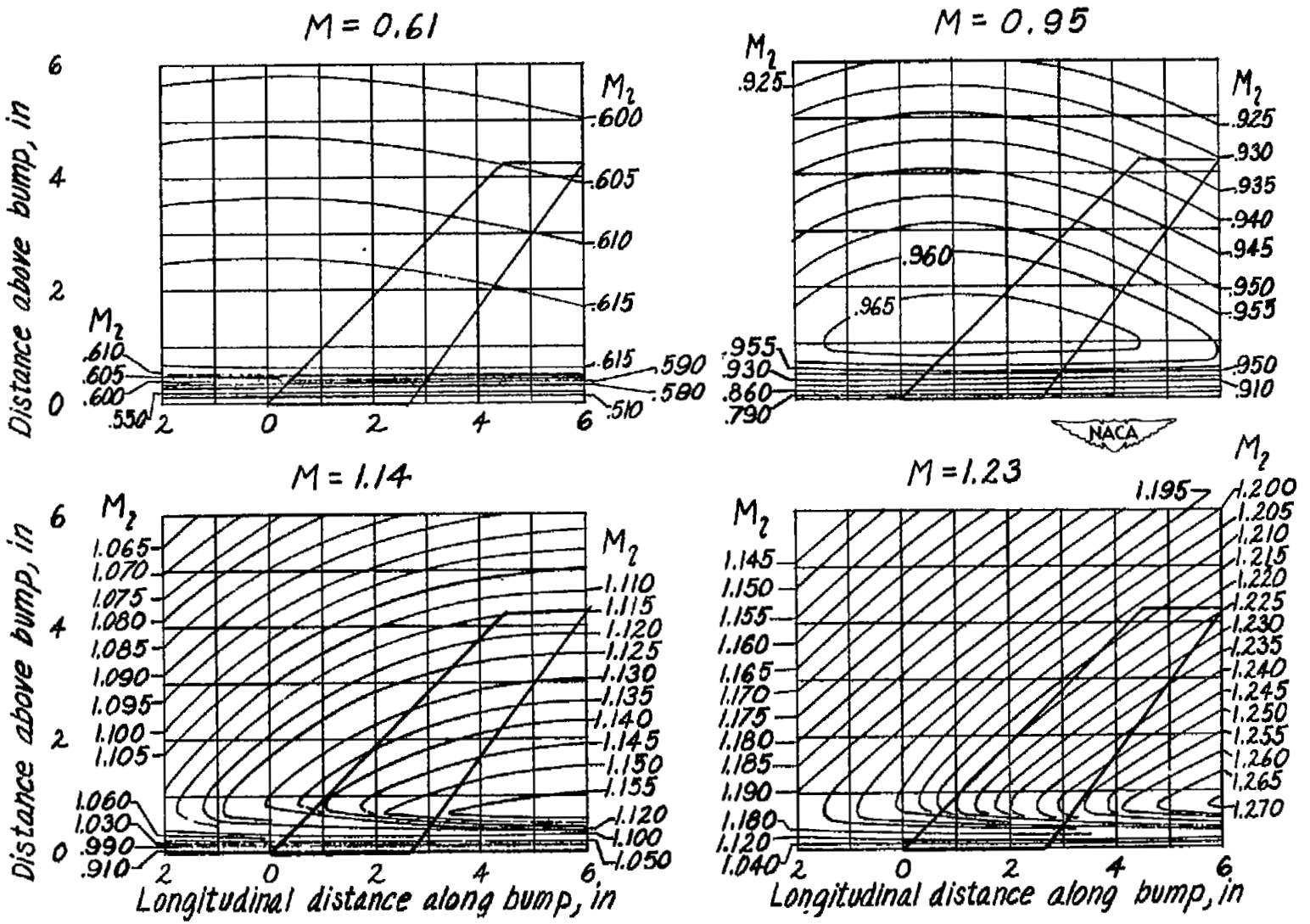

Figure 5.- Typical Mach number contours obtained over the all-movable tail.

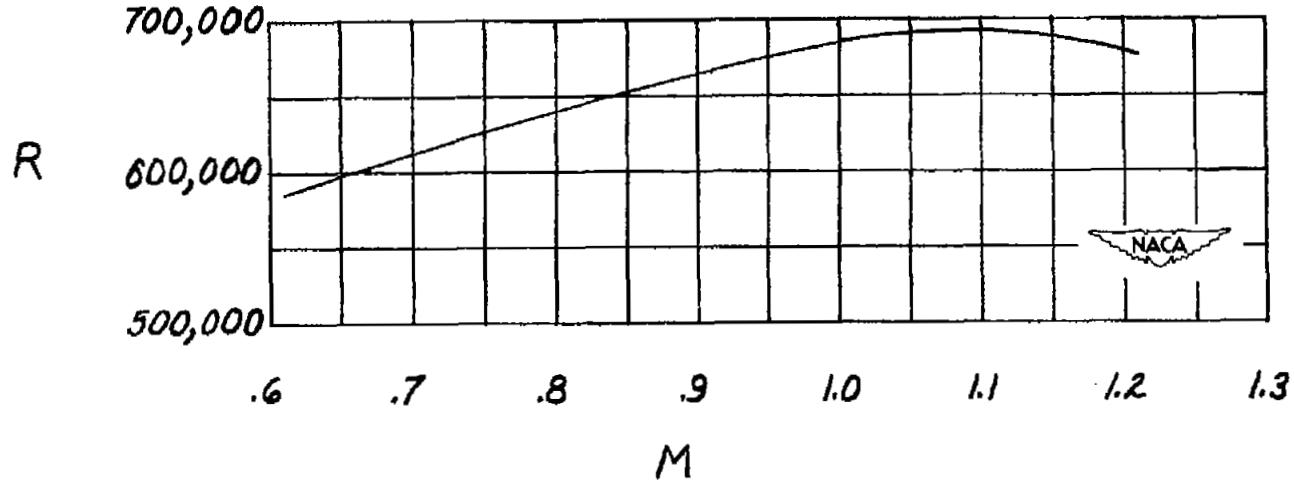

Figure 6.- The average variation of Reynolds number with Mach number for tests of the all-movable tail.

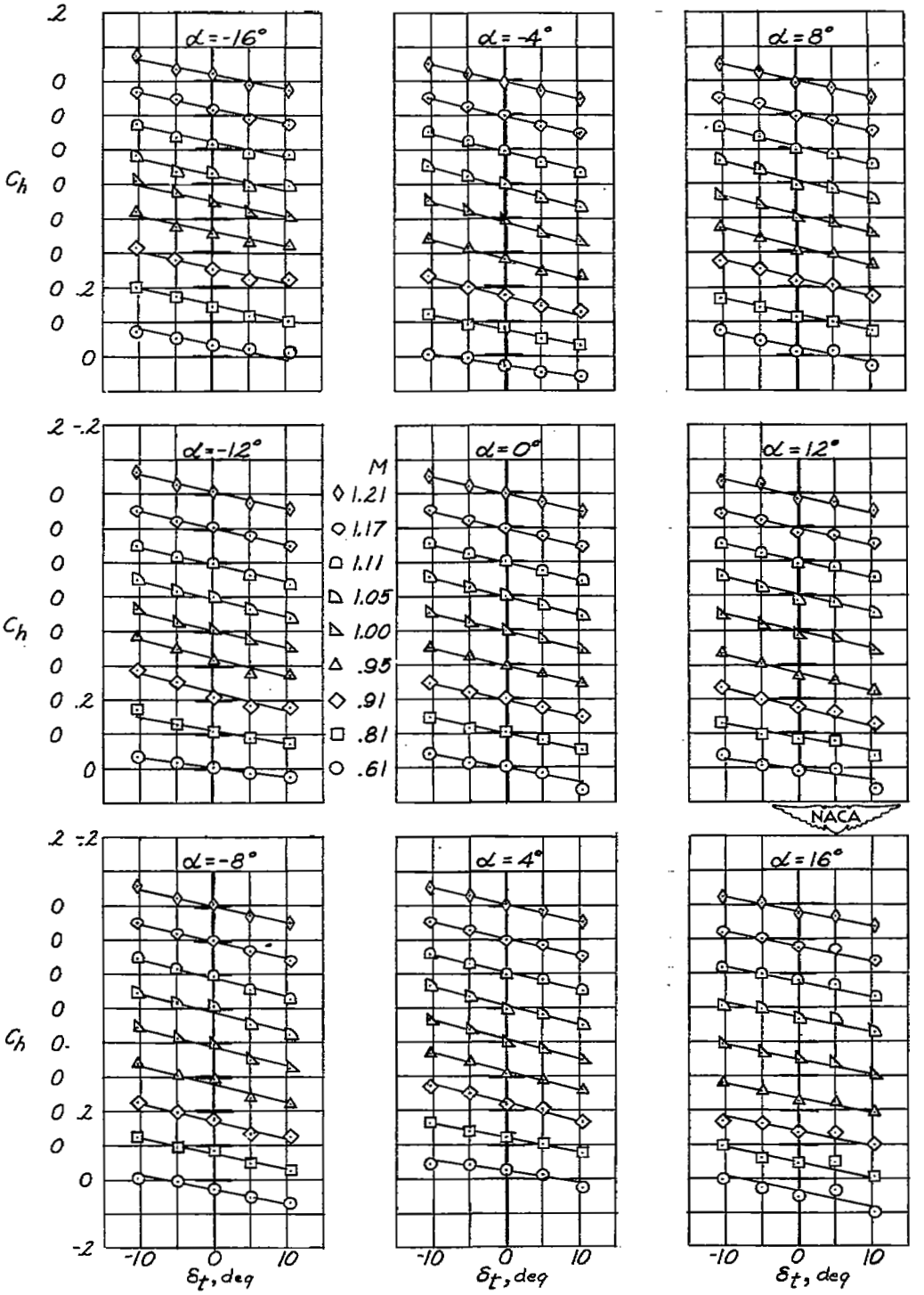

Figure 7.- The variation of hinge-moment and lift coefficients with inset tab deflection for various Mach numbers and angles of attack. $\delta = 0^{\circ}$.

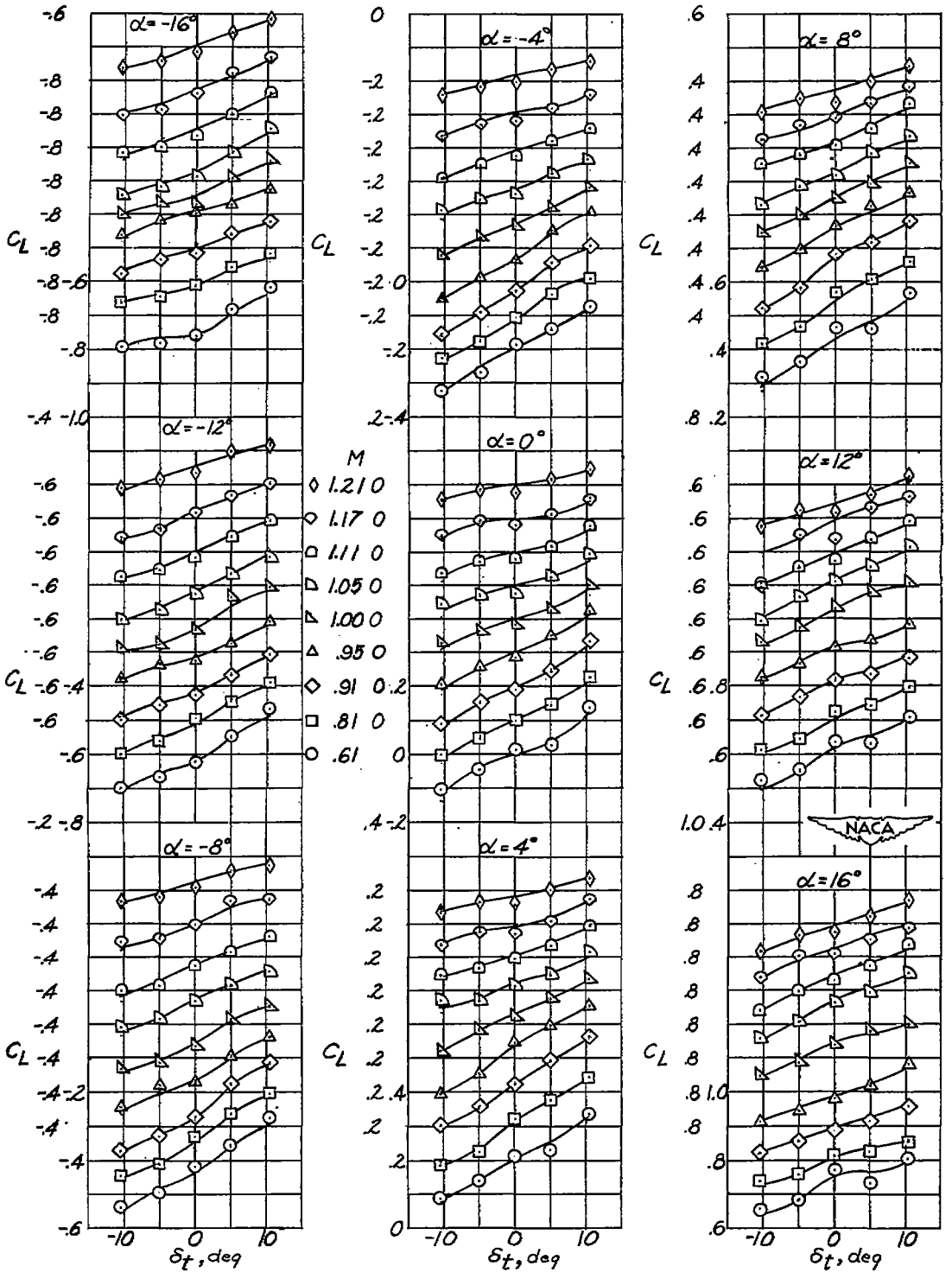

Figure 7.- Concluded.

[redacted]

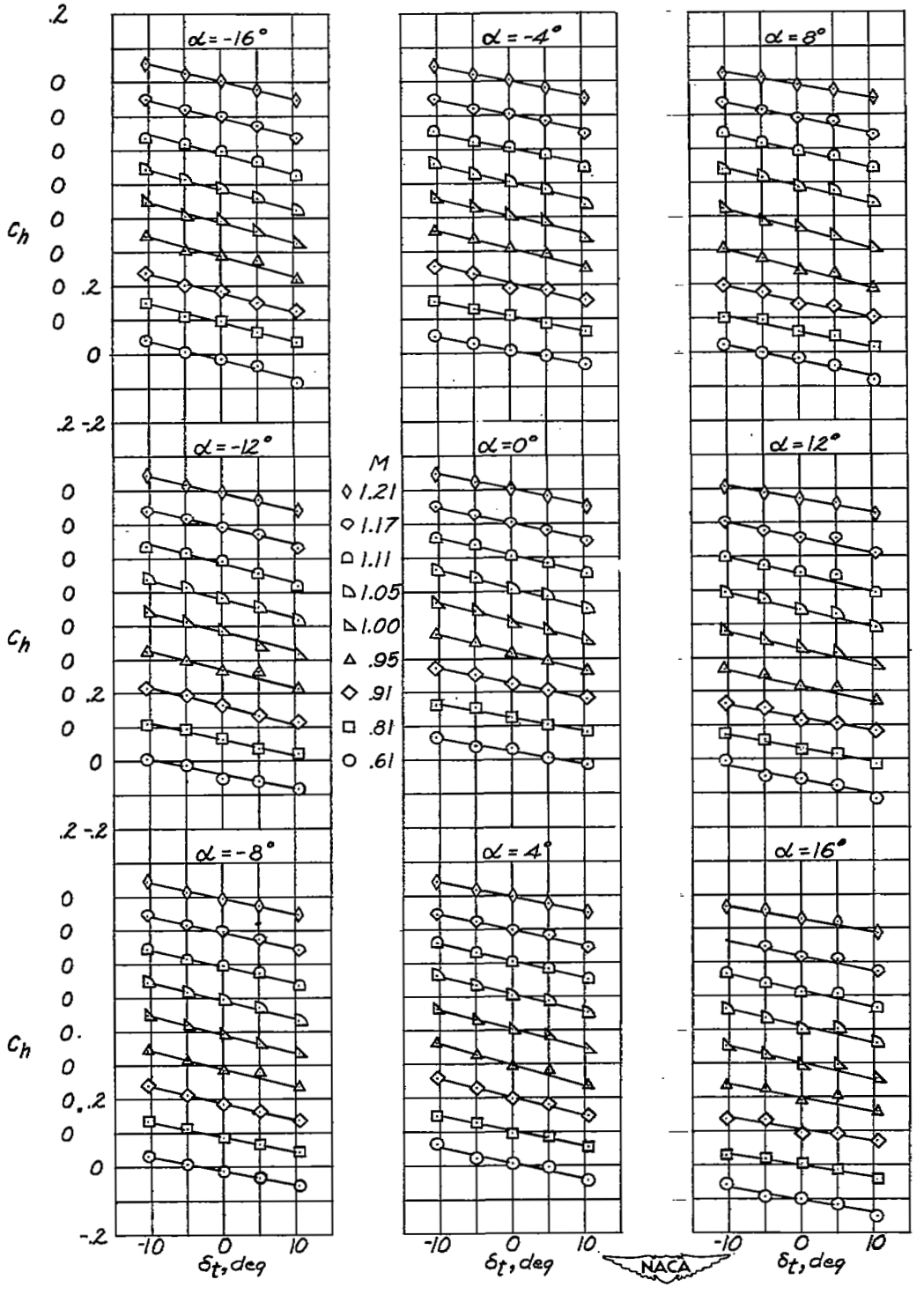

Figure 8.- The variation of hinge-moment and lift coefficients with inset tab deflection for various Mach numbers and angles of attack. $\delta = 10^\circ$.

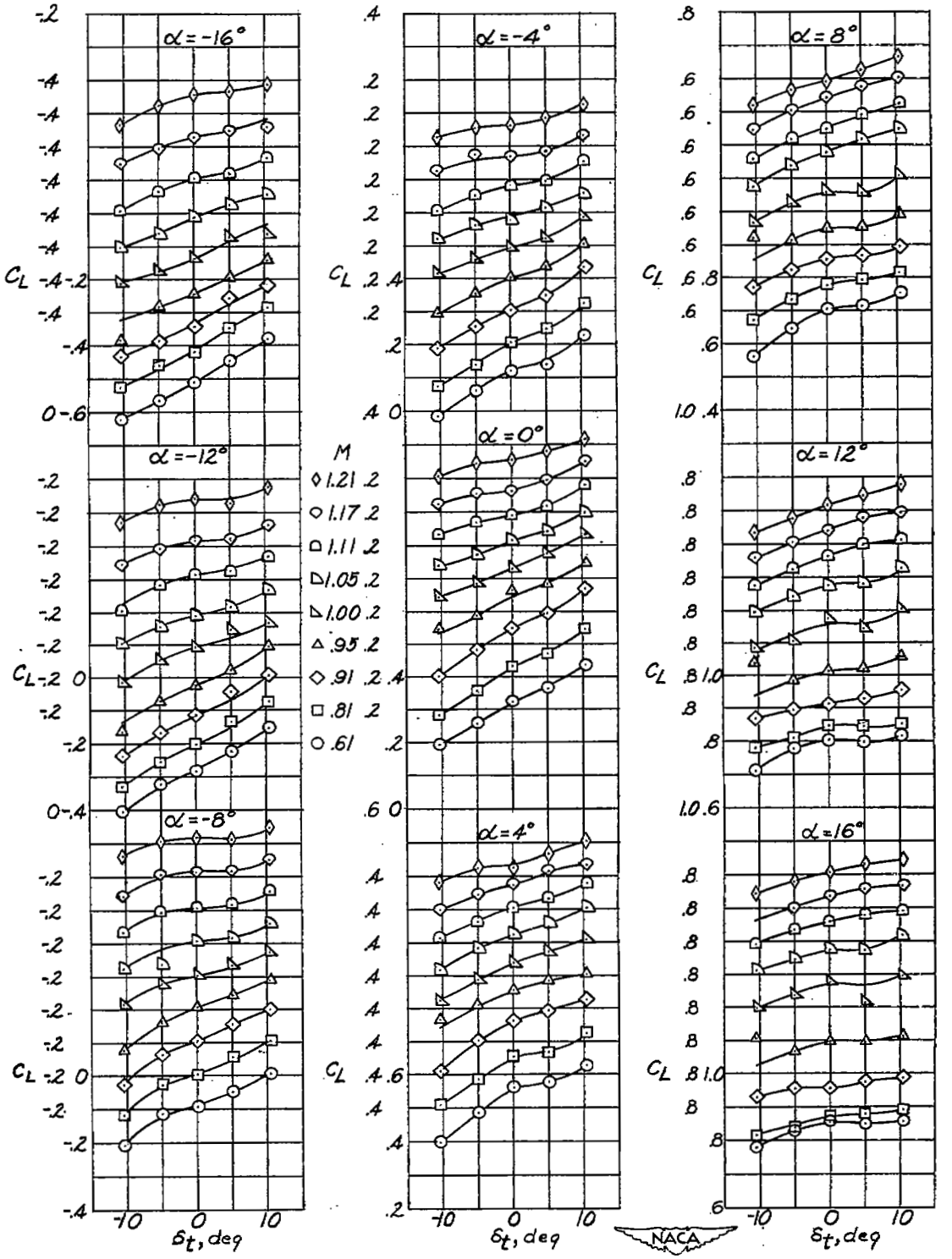

Figure 8.- Concluded.

[redacted]

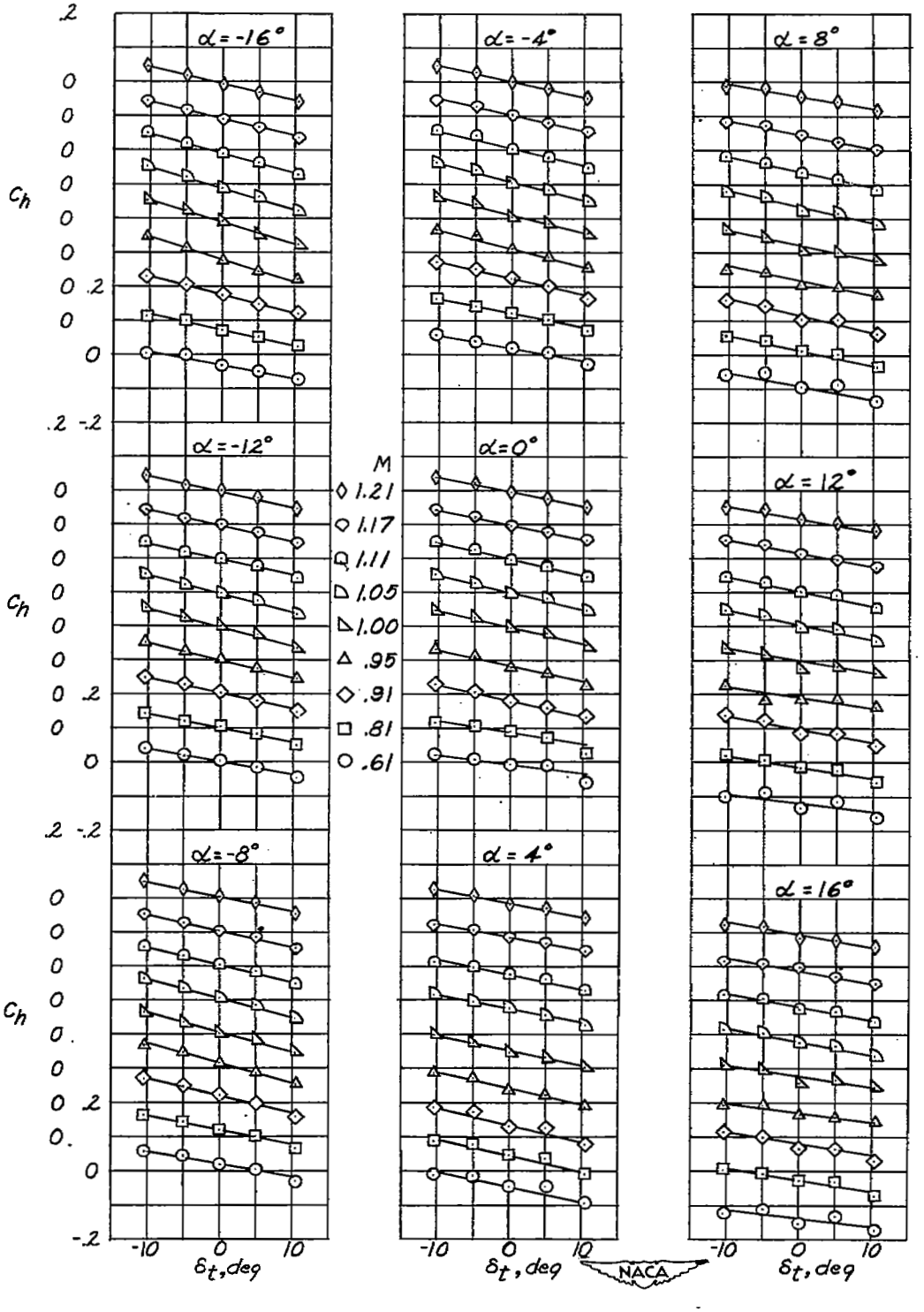

Figure 9.- The variation of hinge-moment and lift coefficients with inset tab deflection for various Mach numbers and angles of attack. $\delta = 20^{\circ}$.

[redacted]

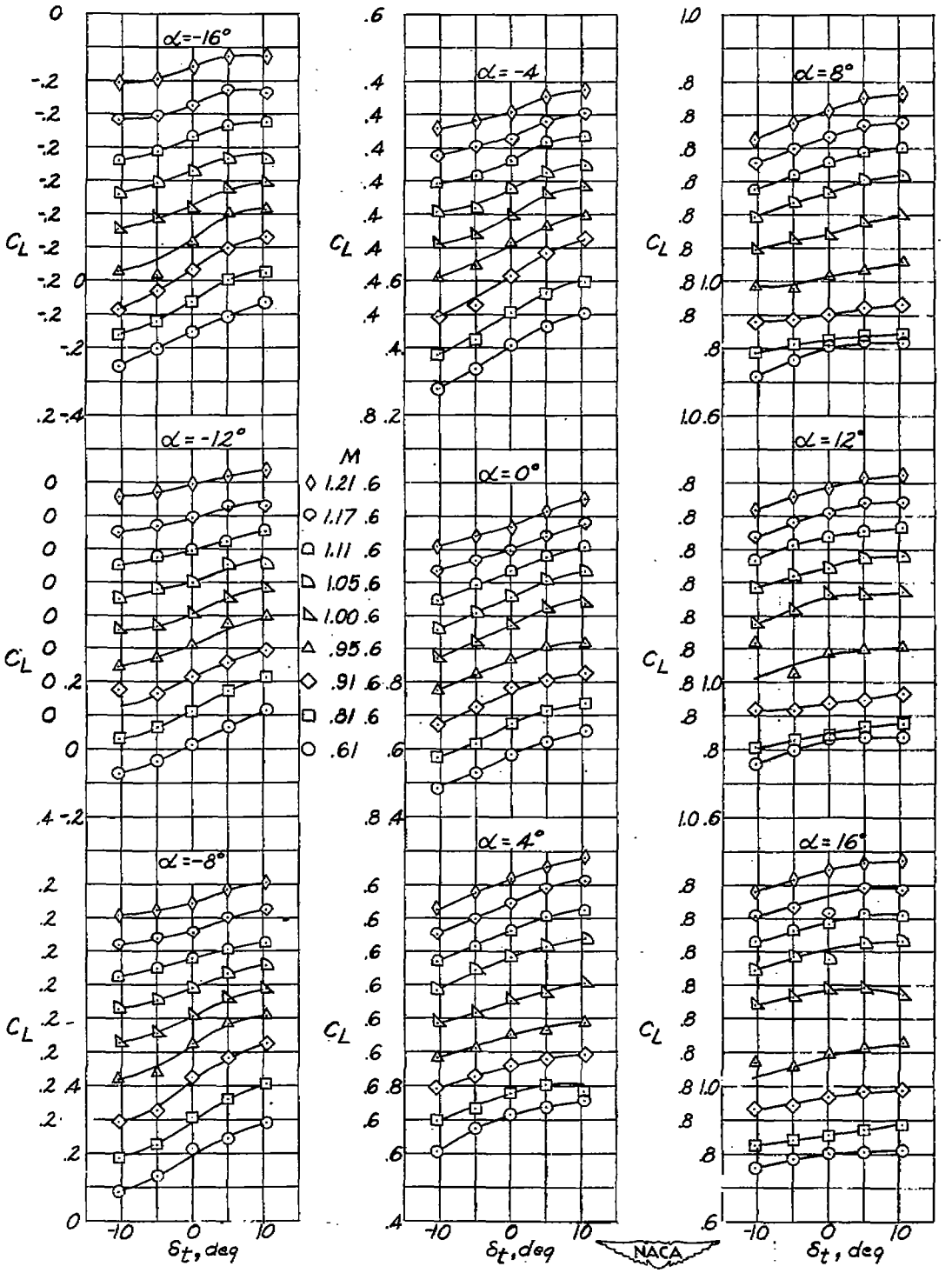

Figure 9.- Concluded.

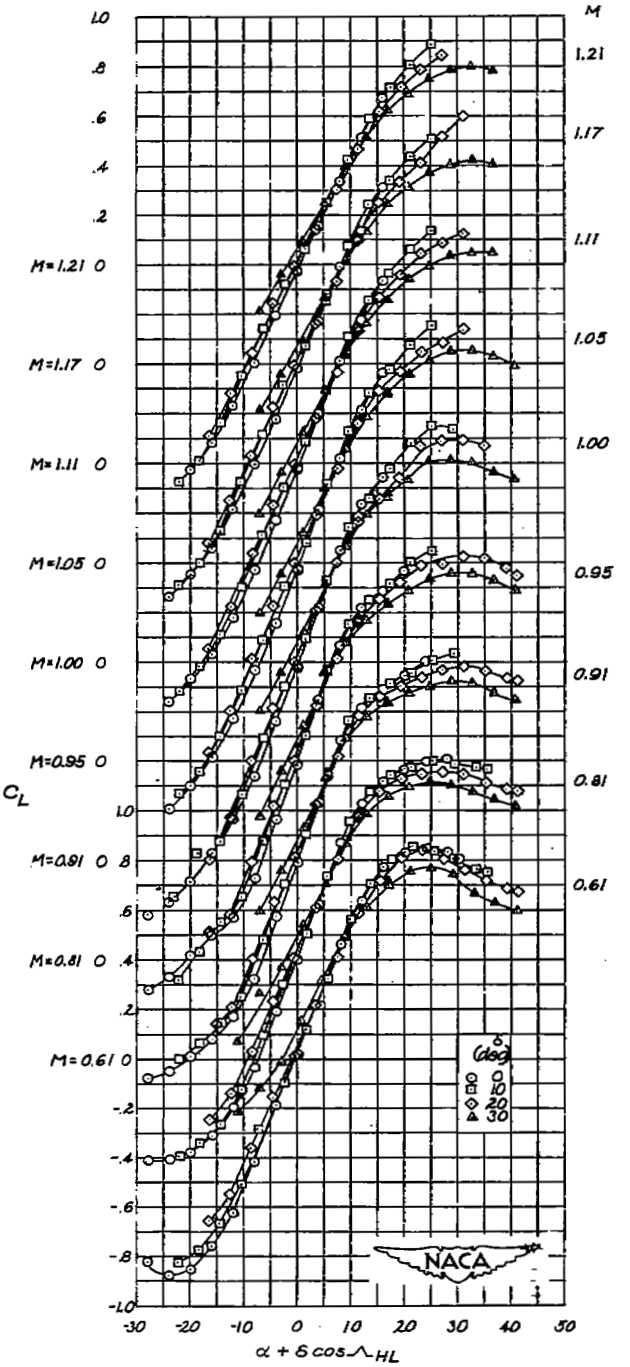

(a) Lift coefficient.

Figure 10.- The variation of lift, pitching-moment, and hinge-moment coefficients with the parameter $\alpha + \delta \cos \Lambda_{HL}$ for the all-movable tail at various tail deflections and Mach numbers. $\delta_t = 0$.

[redacted]

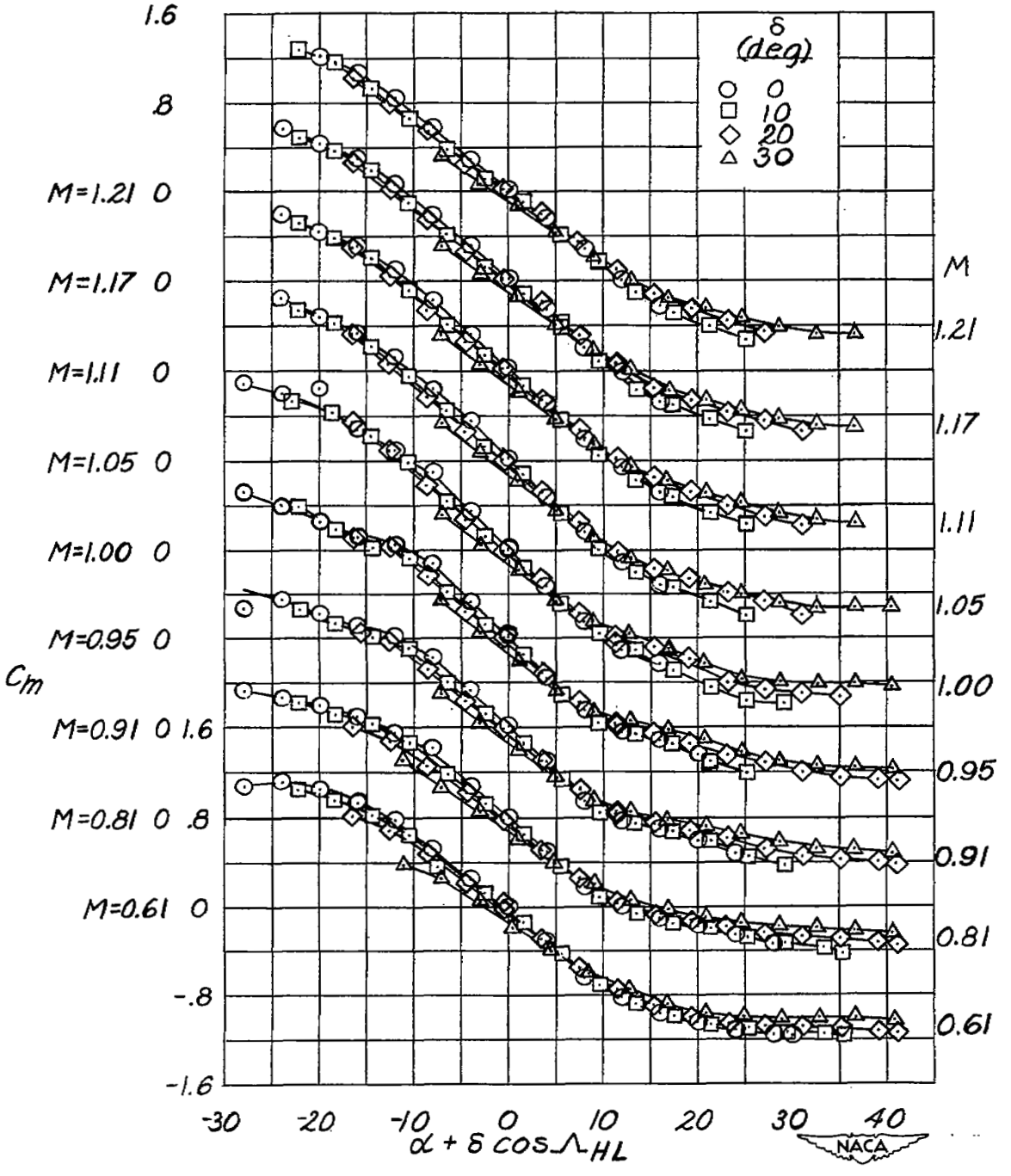

(b) Pitching-moment coefficient.

Figure 10.- Continued.

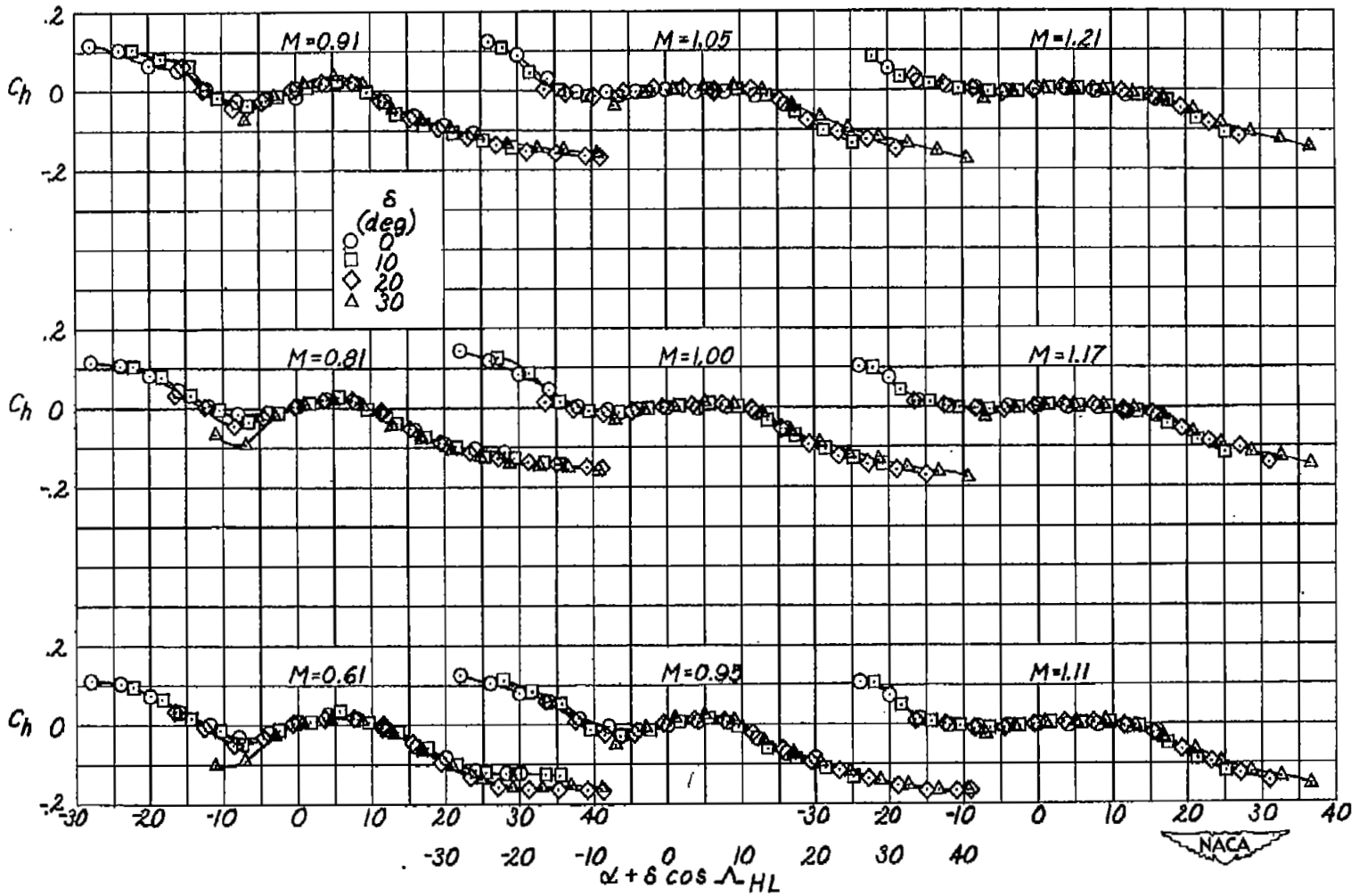

(c) Hinge-moment coefficient.

Figure 10.- Concluded.

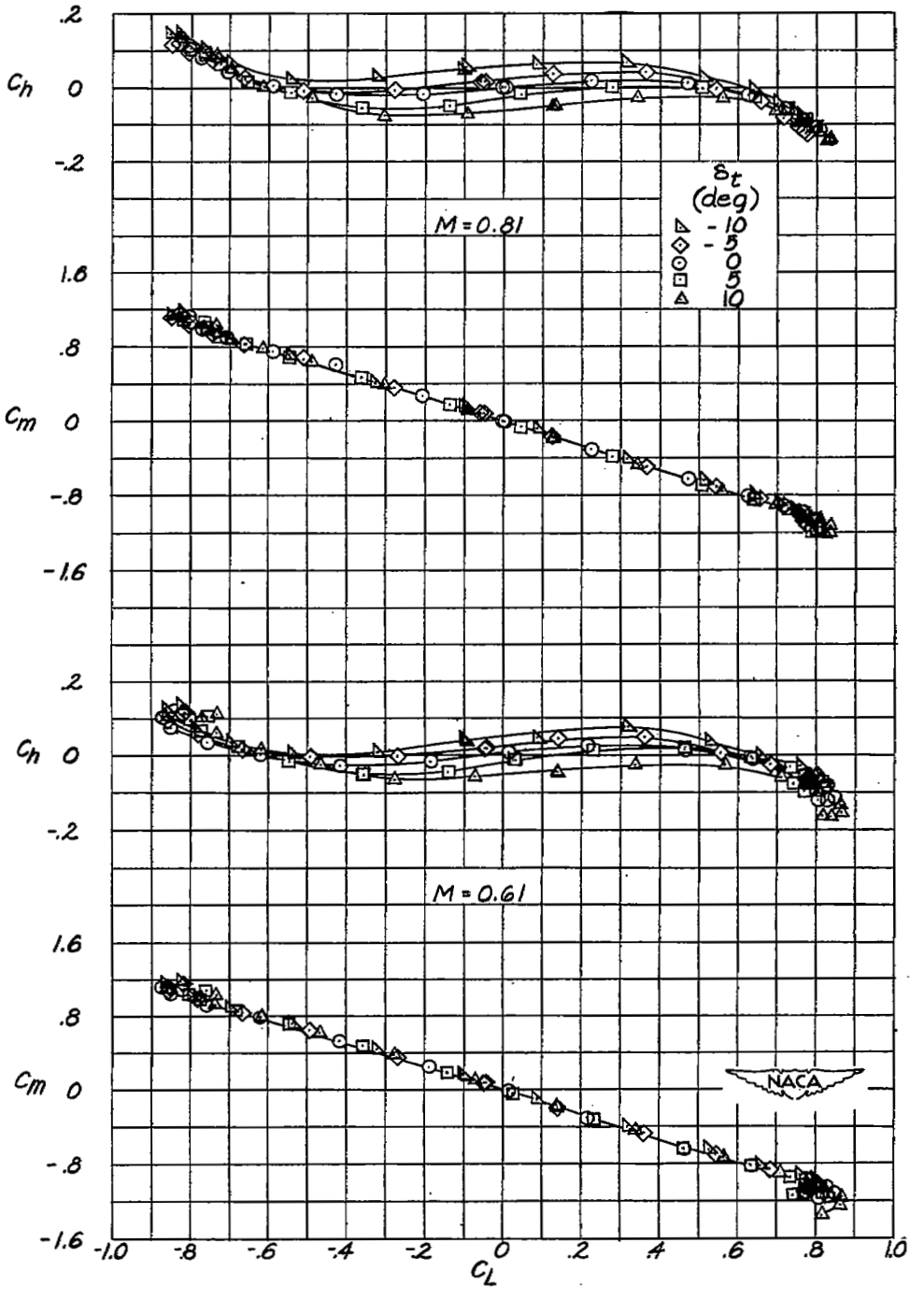

(a) M = 0.61 and 0.81.

Figure 11.- The variation of pitching-moment and hinge-moment coefficients with lift coefficient for various Mach numbers. $\delta = 0^{\circ}$.

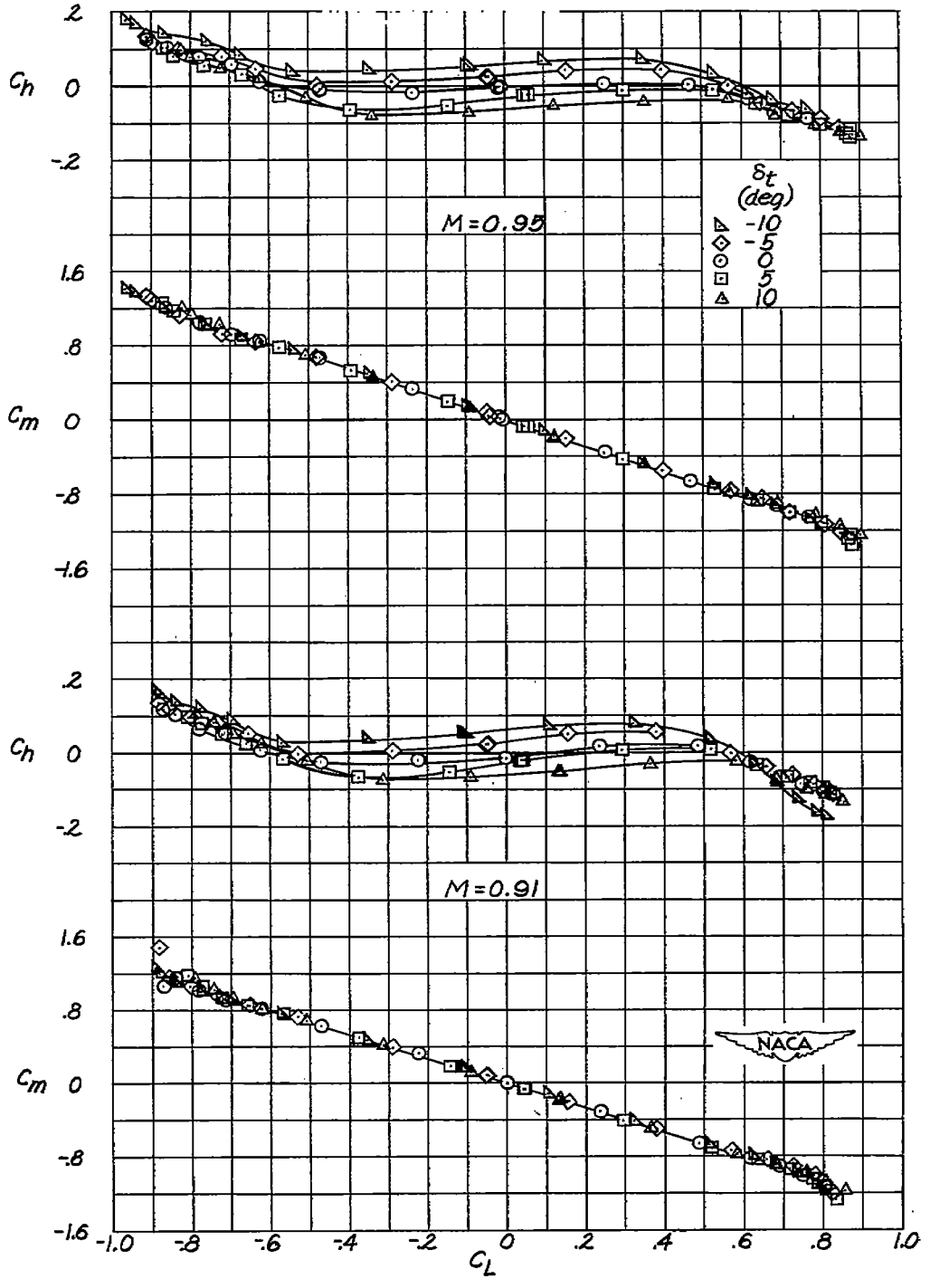

(b) M = 0.91 and 0.95.

Figure 11.- Continued.

[redacted]

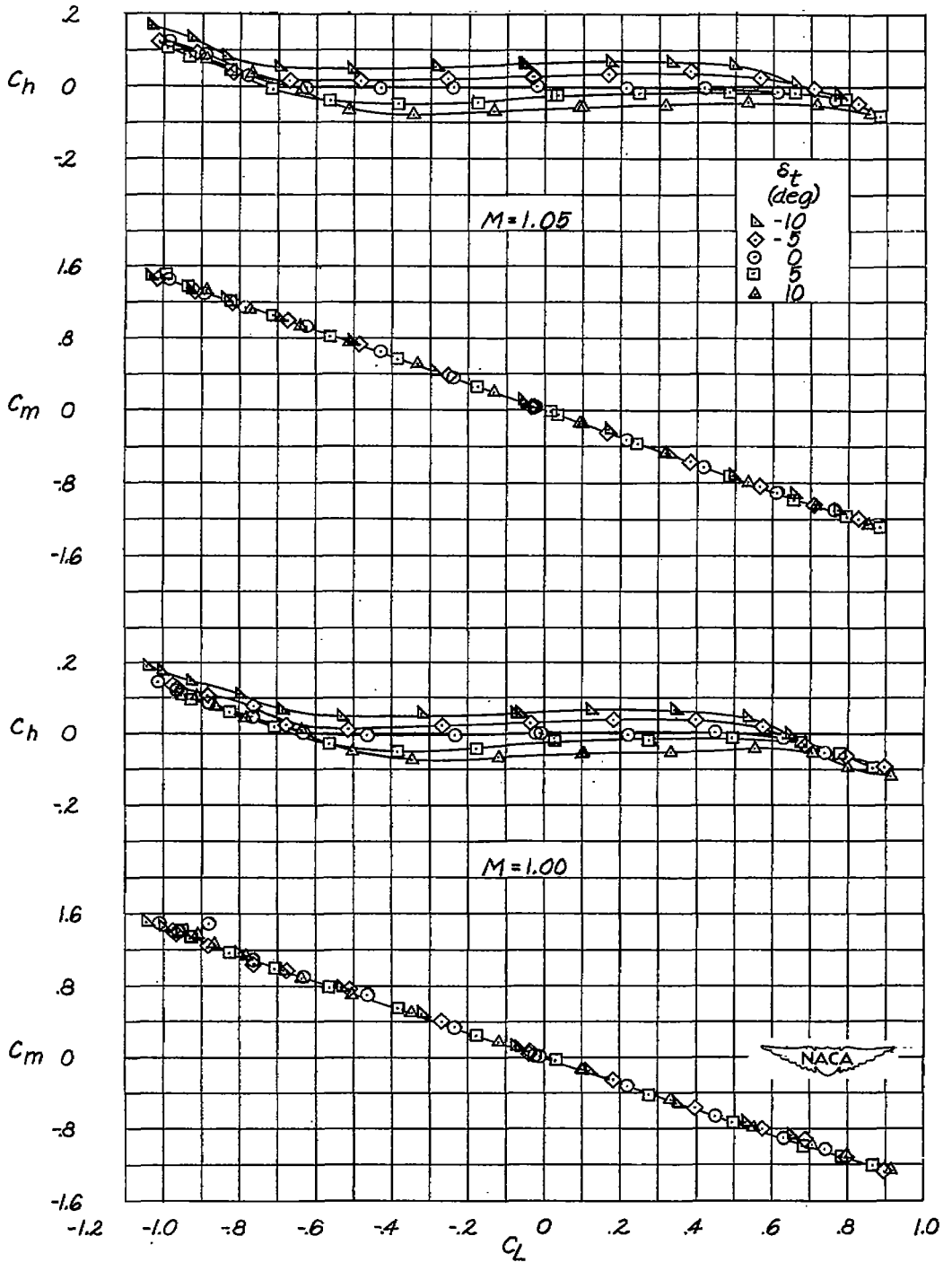

(c) M = 1.00 and 1.05.

Figure 11.- Continued.

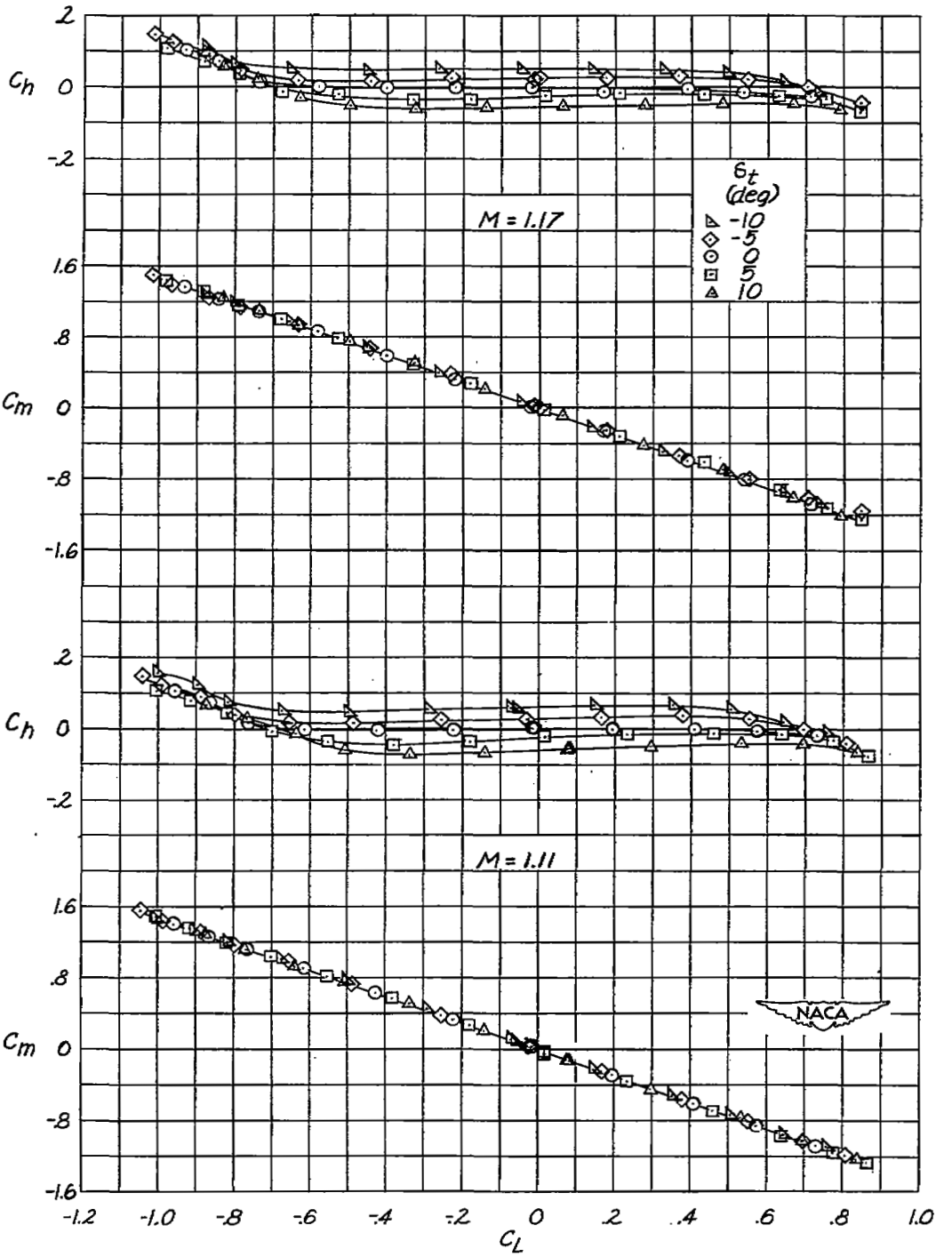

(d) M = 1.11 and 1.17.

Figure 11.- Continued.

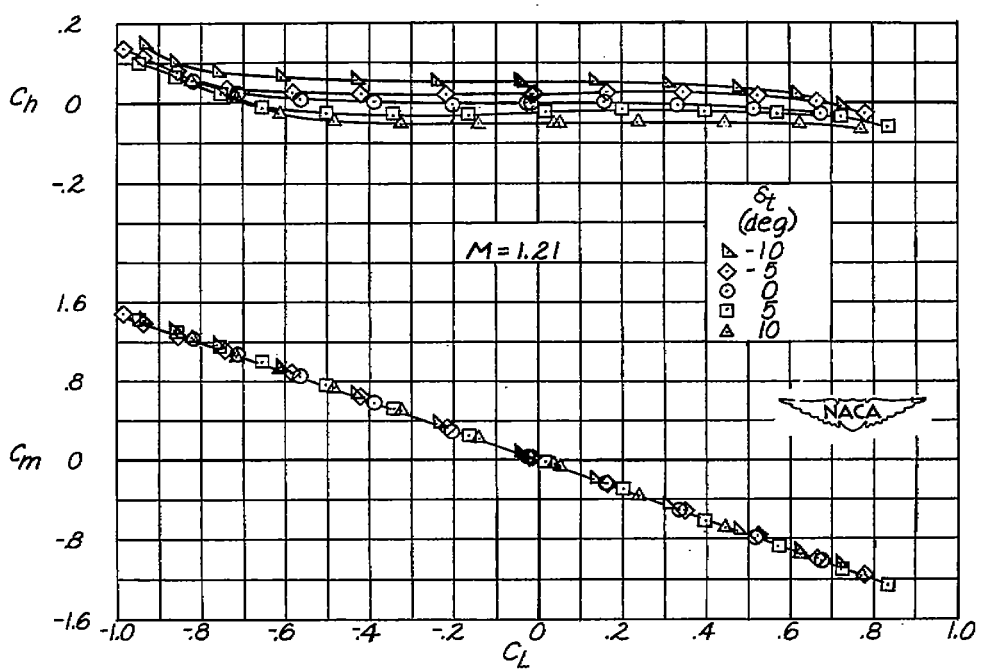

(e) M = 1.21.

Figure 11.- Concluded.

[redacted]

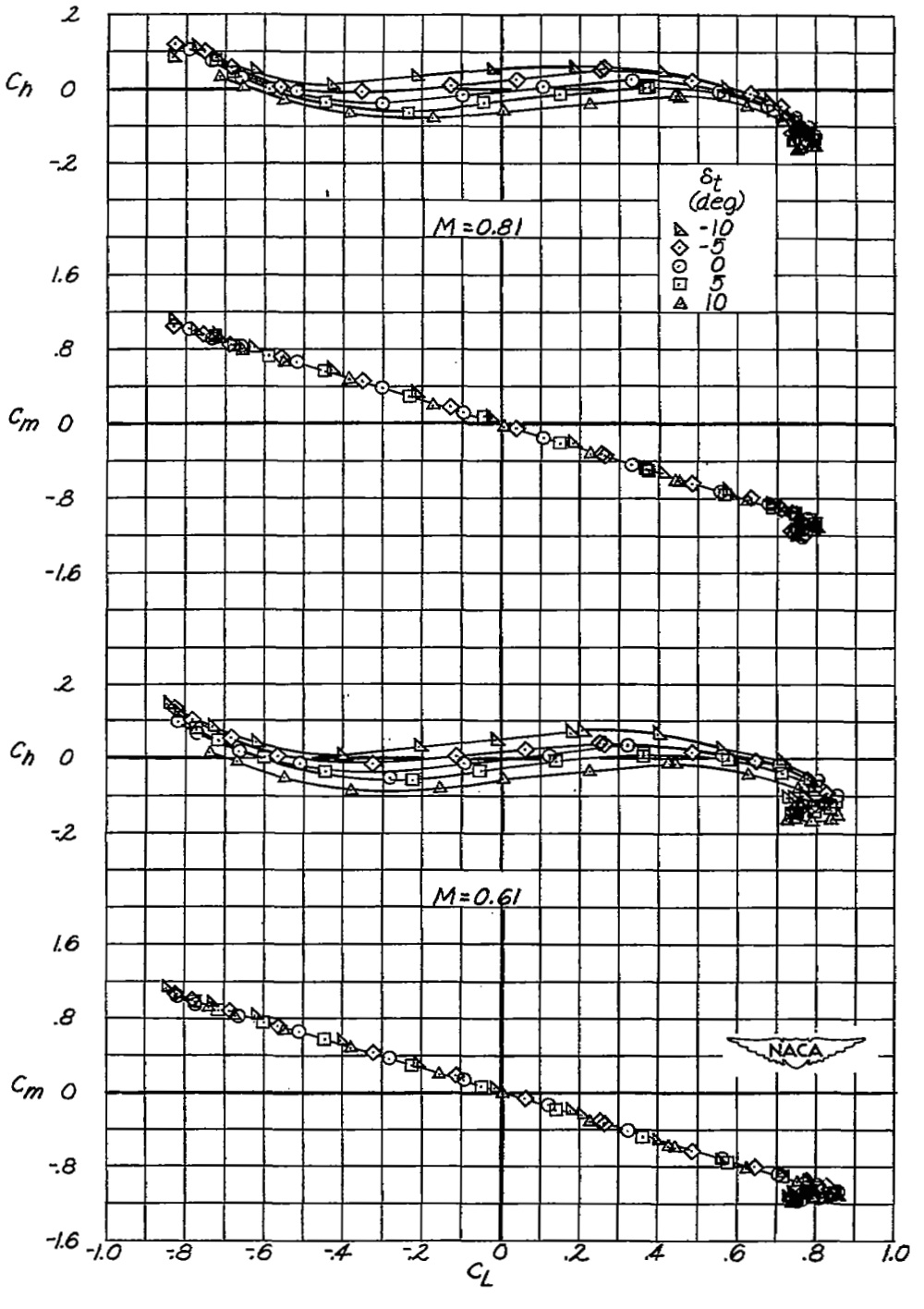

(a) M = 0.61 and 0.81.

Figure 12.- The variation of pitching-moment and hinge-moment coefficients with lift coefficient for various Mach numbers. $\delta = 10^{\circ}$.

[redacted]

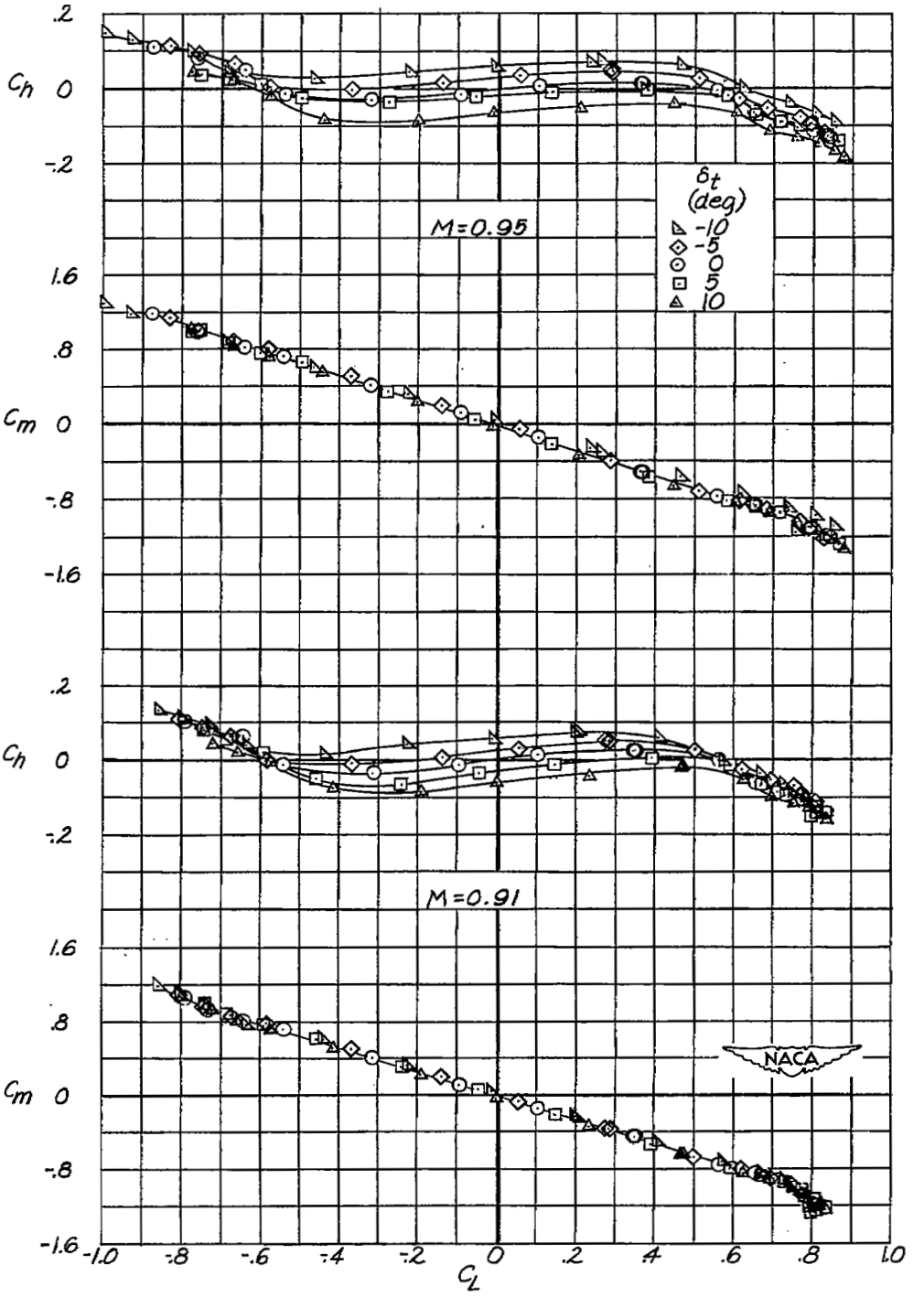

(b) M = 0.91 and 0.95.

Figure 12.- Continued.

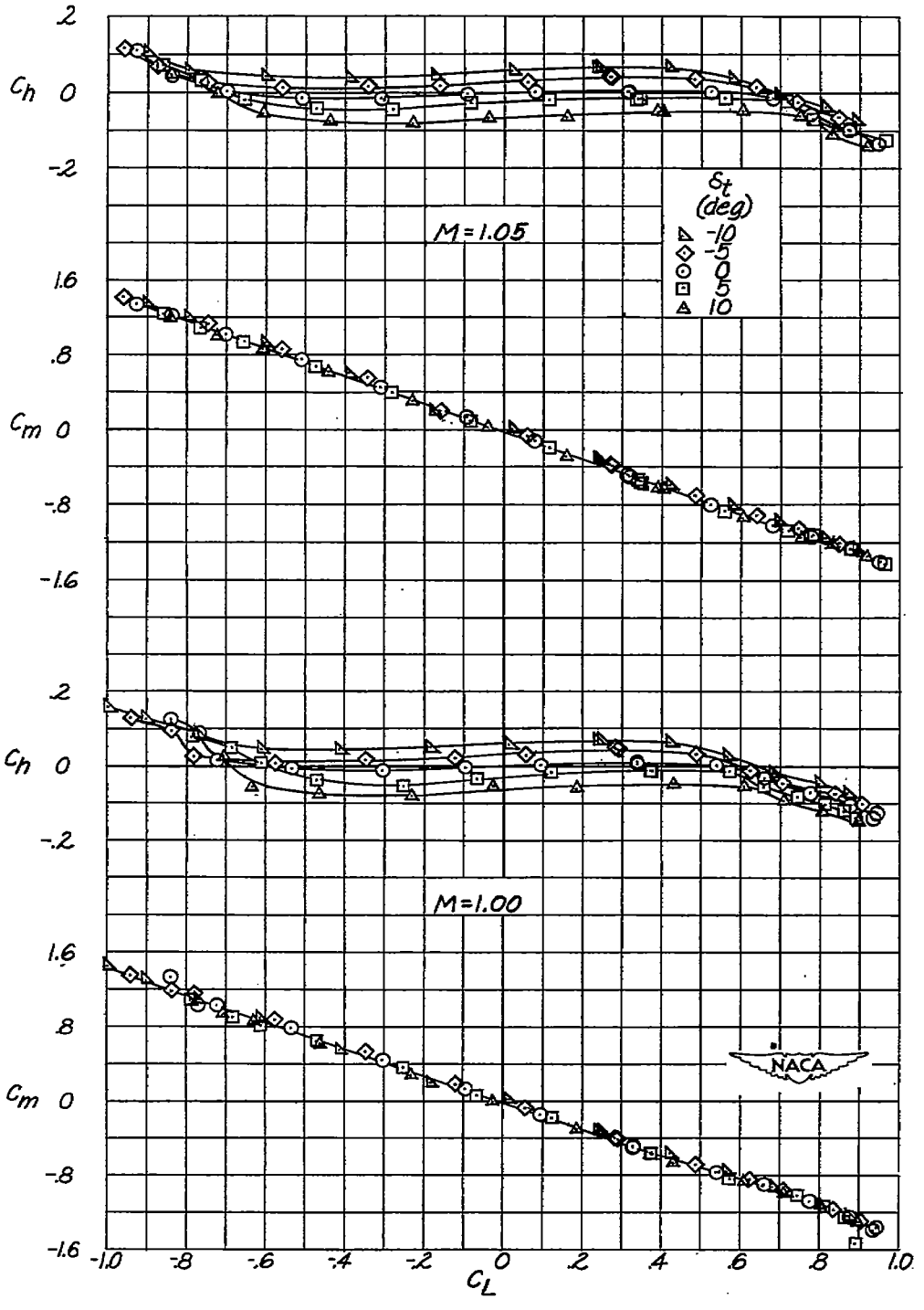

(c) M = 1.00 and 1.05.

Figure 12.- Continued.

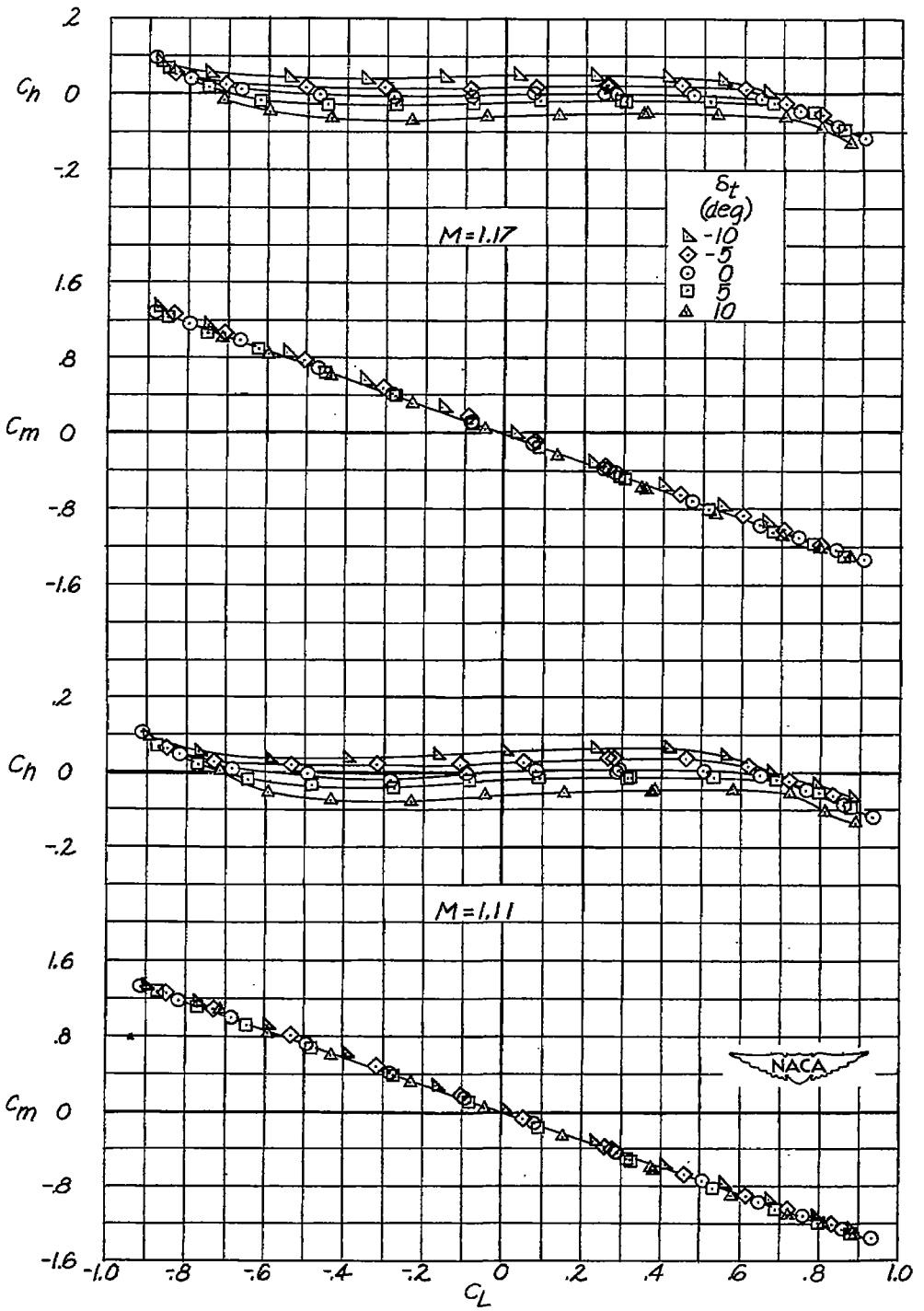

(d) M = 1.11 and 1.17.

Figure 12.- Continued.

[redacted]

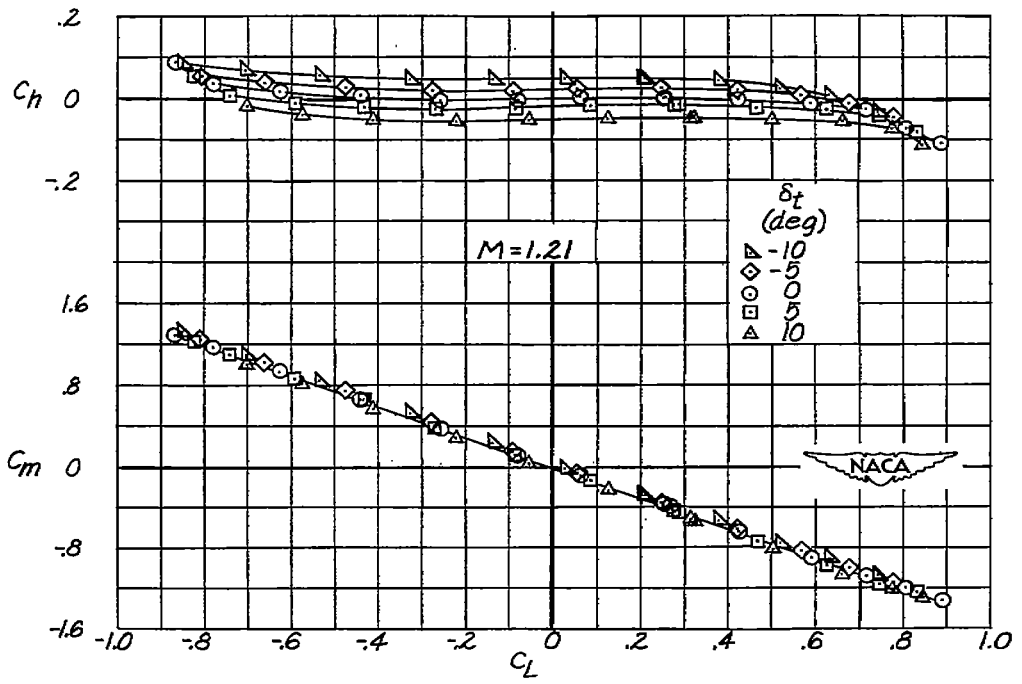

(e) M = 1.21.

Figure 12.- Concluded.

[redacted]

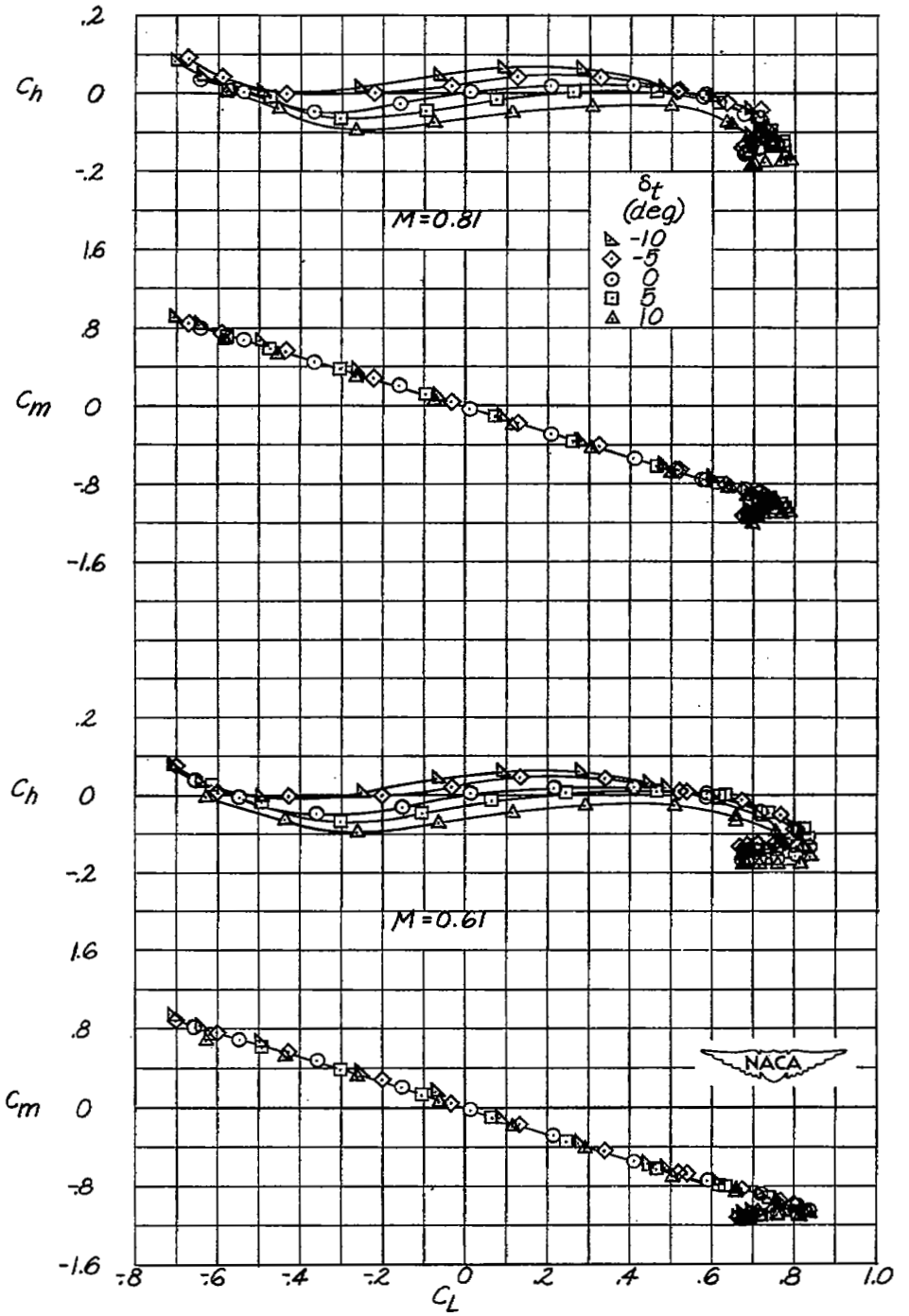

(a) M = 0.61 and 0.81.

Figure 13.- The variation of pitching-moment and hinge-moment coefficients with lift coefficient for various Mach numbers. $\delta = 20^{\circ}$.

[redacted]

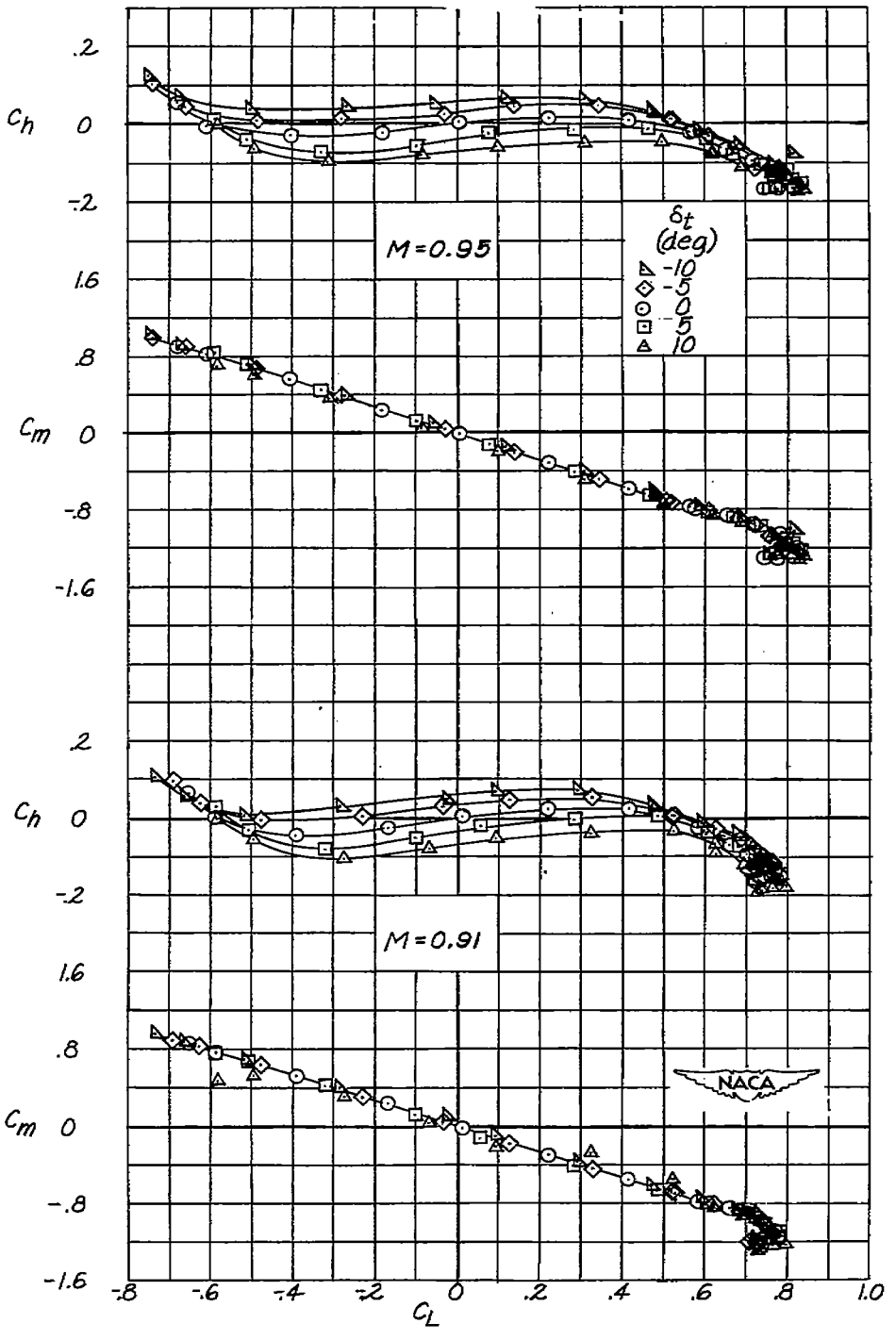

(b) M = 0.91 and 0.95.

Figure 13.- Continued.

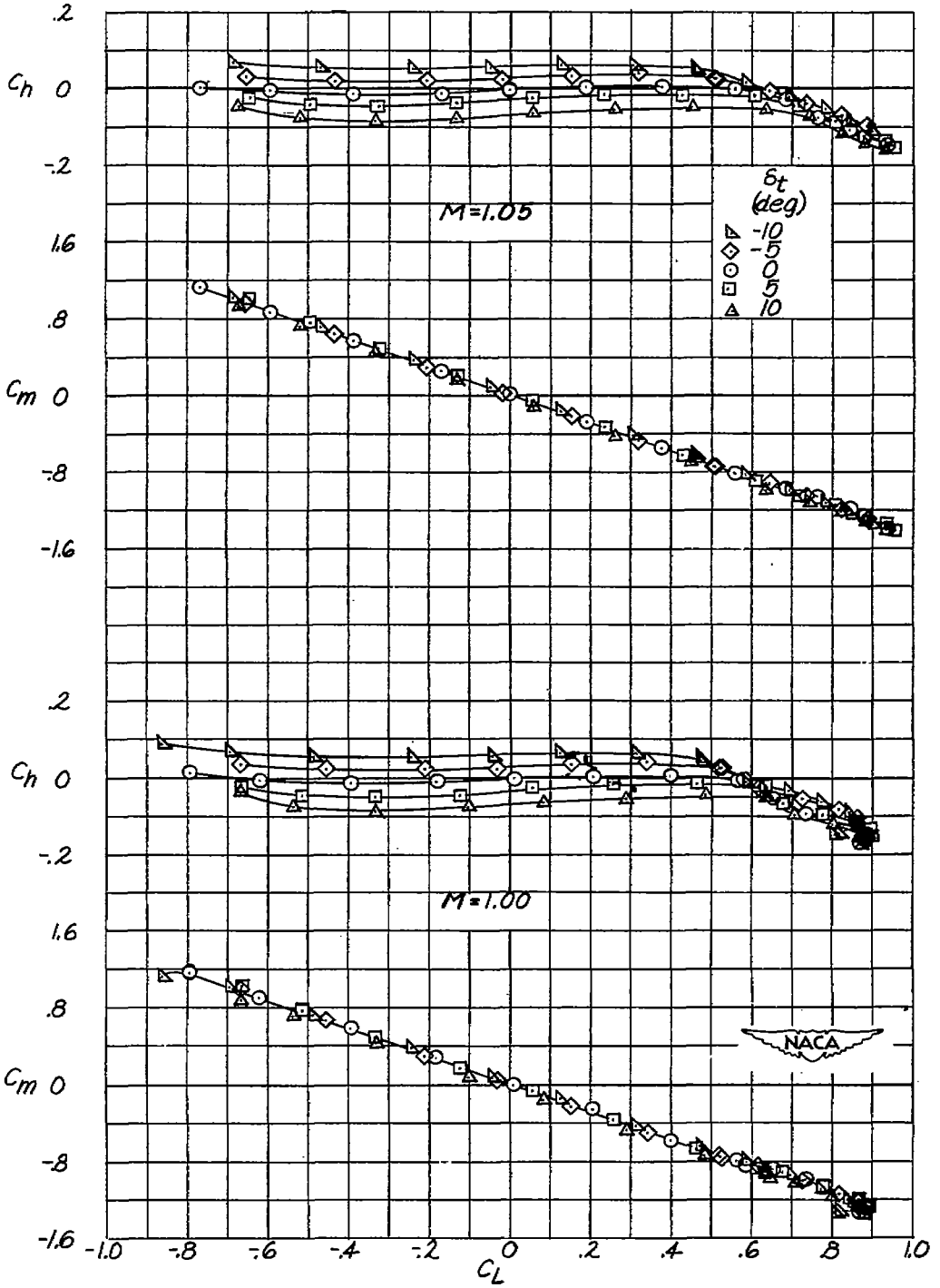

(c) M = 1.00 and 1.05.

Figure 13.- Continued.

[redacted]

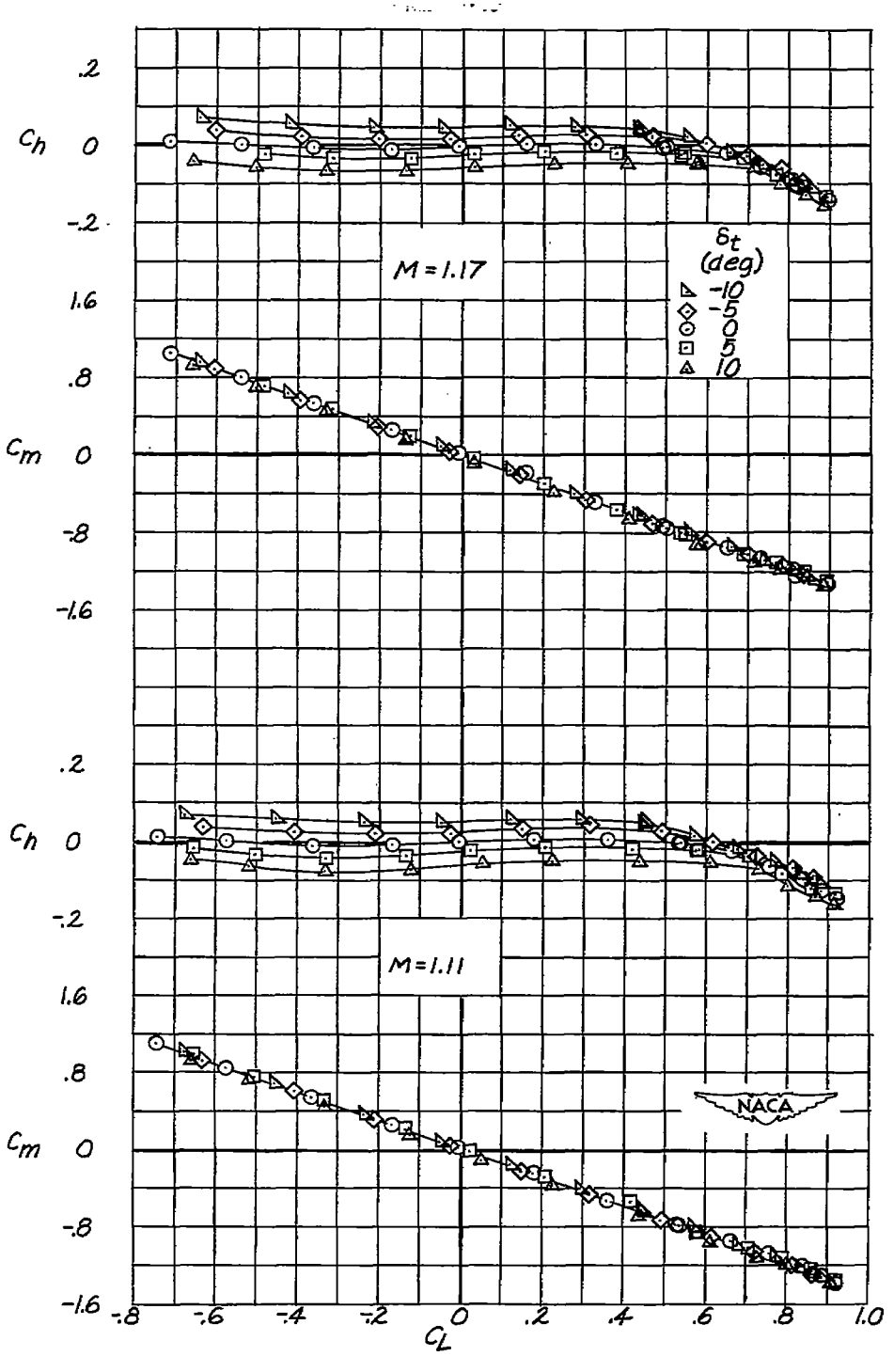

(d) M = 1.11 and 1.17.

Figure 13.- Continued.

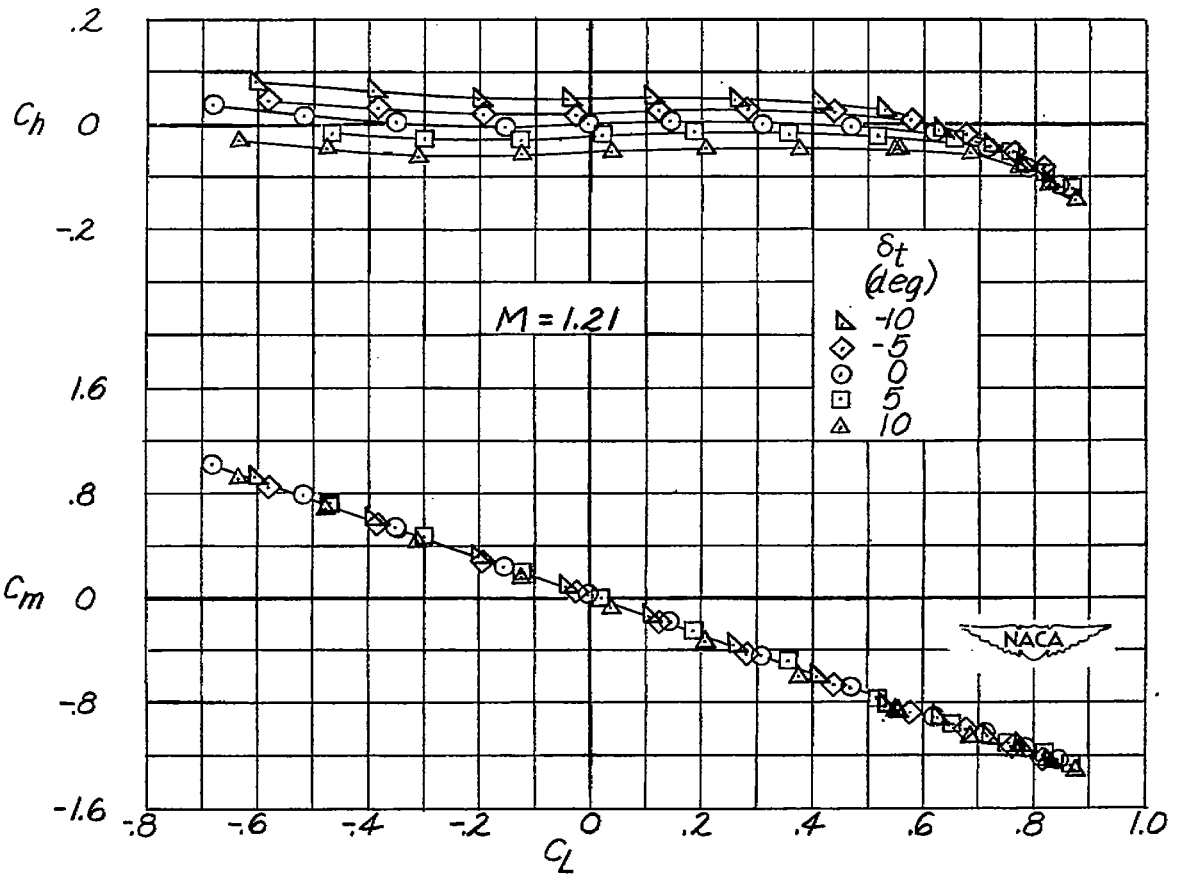

(e) M = 1.21.

Figure 13.- Concluded.

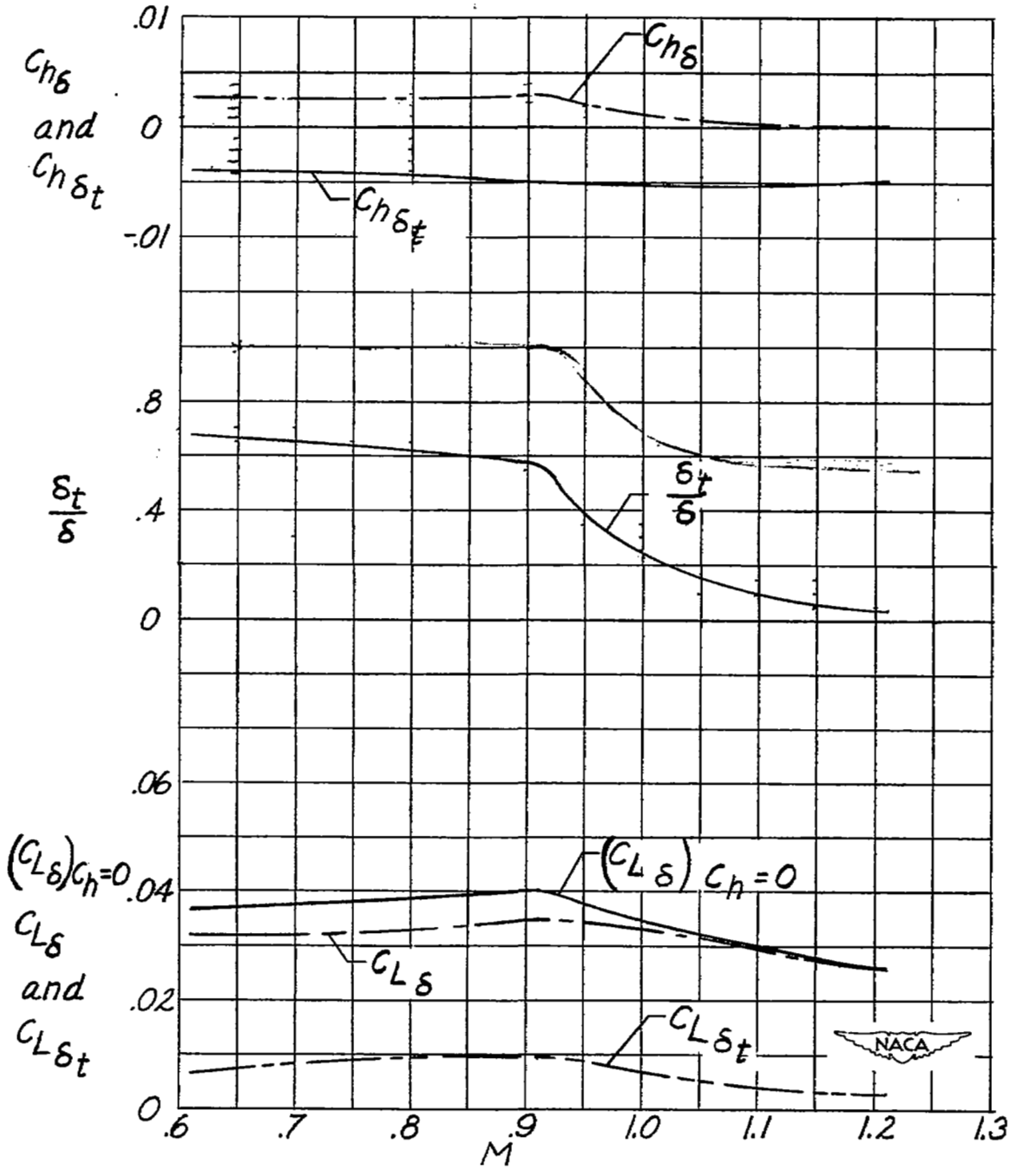

Figure 14.- The variation of the control parameters C_{h_δ}, $C_{h_{\delta_t}}$, δ_t/δ, $(C_{L_\delta})_{C_h=0}$, C_{L_δ}, and $C_{L_{\delta_t}}$ with Mach number.

[redacted]

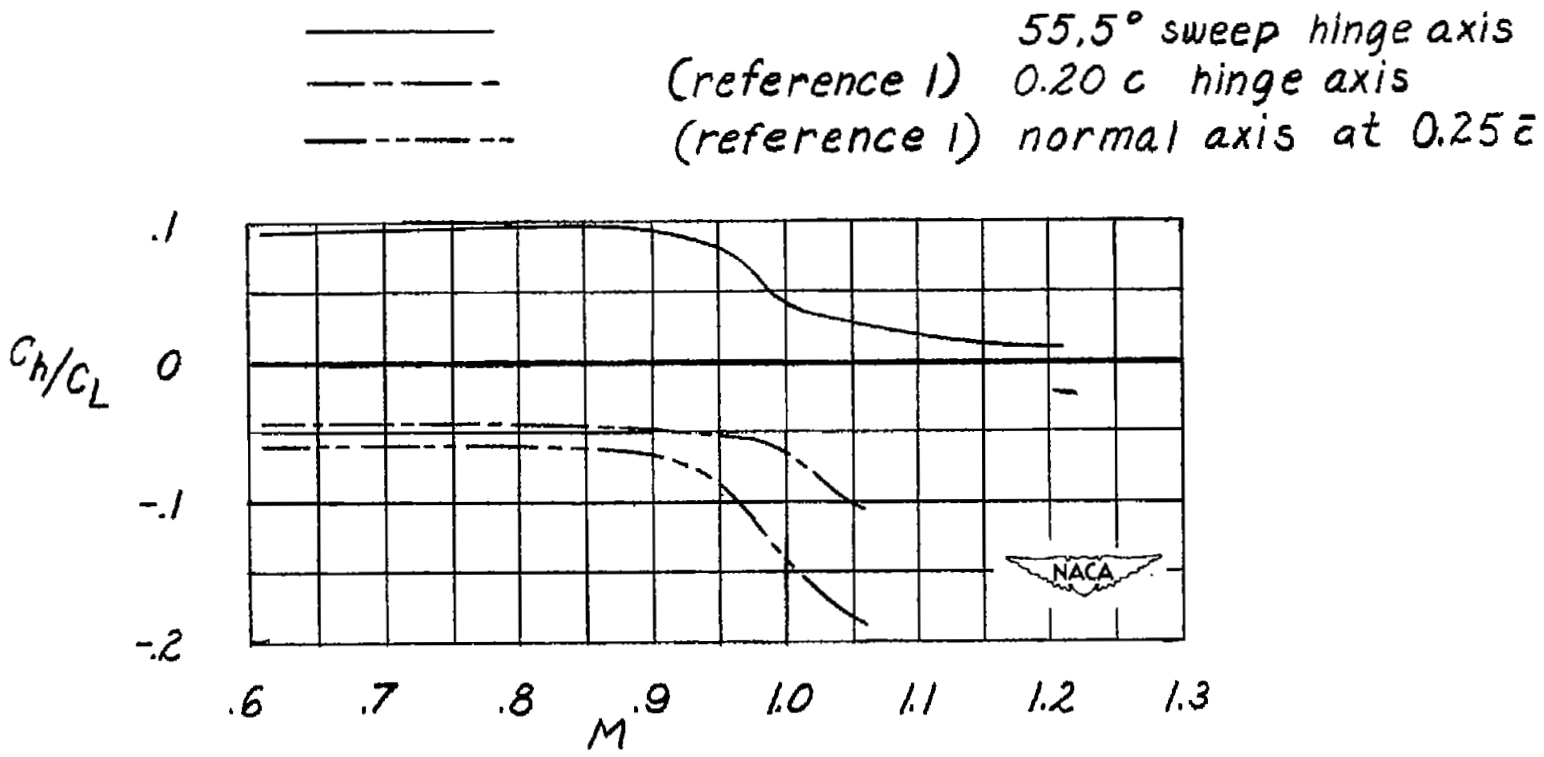

Figure 15.- The variation of the parameter C_h/C_L with Mach number for the 55.5° sweep hinge axis, the 0.20c sweep hinge axis, and the normal axis for the movable tail. (Measured near zero lift.)

NACA-Langley - 8-20-53 - 225